**Supporting Information for**

# Copper chloride complexes with substituted 4′-phenyl-terpyridine ligands: synthesis, characterization, antiproliferative activities and DNA interactions

Jiahe Li, [a,b,c] Hao Yan, [d] Zhiyuan Wang, [a] Rongping Liu, [a] Baomei Luo, [a] Dengfeng Yang, [e] Hailan Chen,*[d] Lixia Pan*[b] and Zhen Ma*[a,c]

[a] School of Chemistry and Chemical Engineering, Guangxi University, 530004, Nanning, Guangxi, People's Republic of China. E-mail: mzmz2009@sohu.com.

[b] National Engineering Research Center for Non-Food Biorefinery, State Key Laboratory of Non-Food Biomass and Enzyme Technology, Guangxi Academy of Sciences, Nanning 530007, Guangxi, People's Republic of China. E-mail: panlixia@gxas.cn.

[c] Centro de Química Estrutural, Instituto Superior Técnico, Universidade de Lisboa, Av. Rovisco Pais, 1049-001, Lisbon, Portugal.

[d] School of Animal Science and Technology, Guangxi University, 530004, Nanning, Guangxi, People's Republic of China. E-mail: hlchen319@163.com.

[e] Guangxi Key Laboratory of Marine Natural Products and Combinatorial Biosynthesis Chemistry, Guangxi Beibu Gulf Marine Research Center, Guangxi Academy of Sciences, Nanning 530007, Guangxi, People's Republic of China.

# INDEX

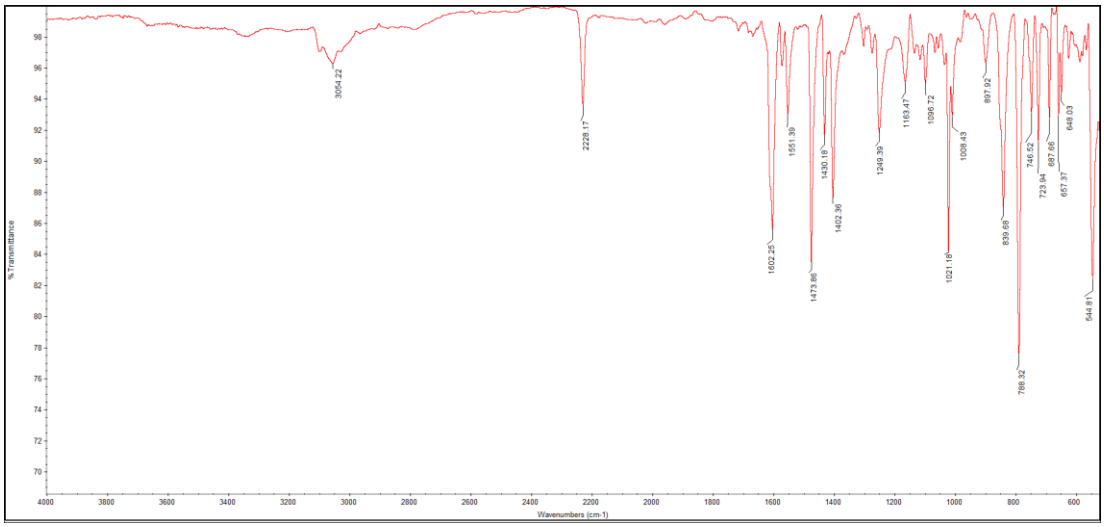


**Figure S1** The IR spectrum of compound **2**.

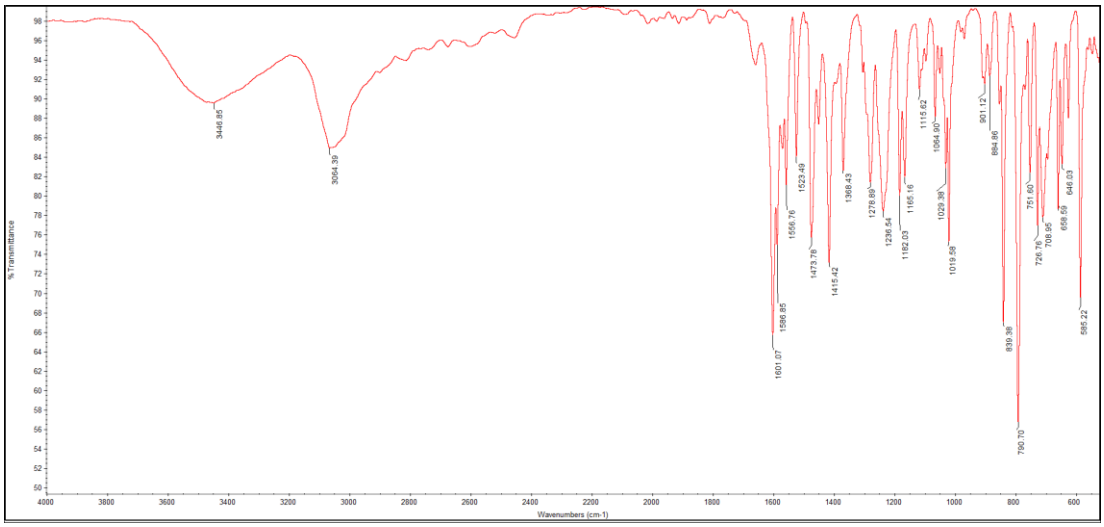


**Figure S2** The IR spectrum of compound **3**.

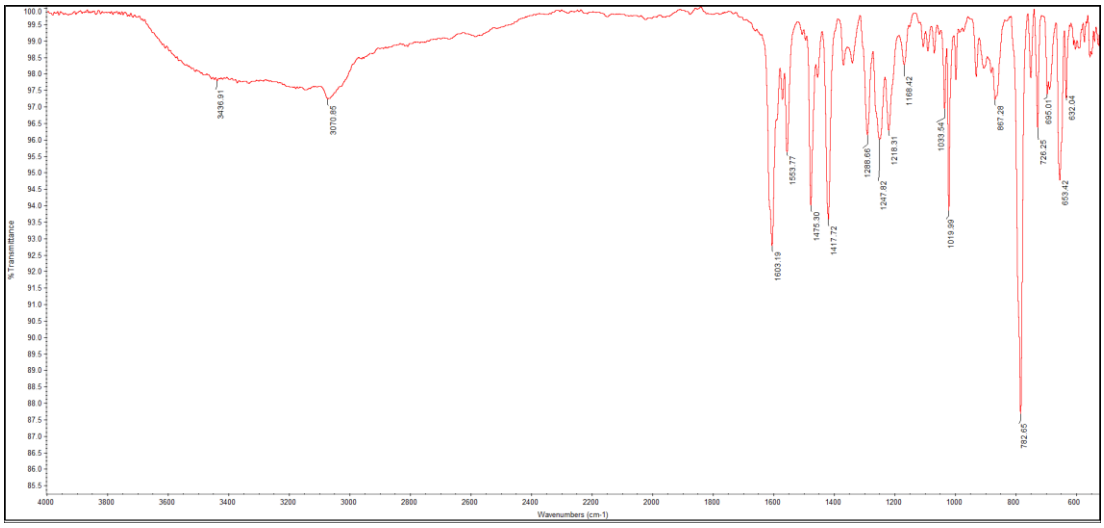


**Figure S3** The IR spectrum of compound **4**.


**Figure S4** The IR spectrum of compound **5**.

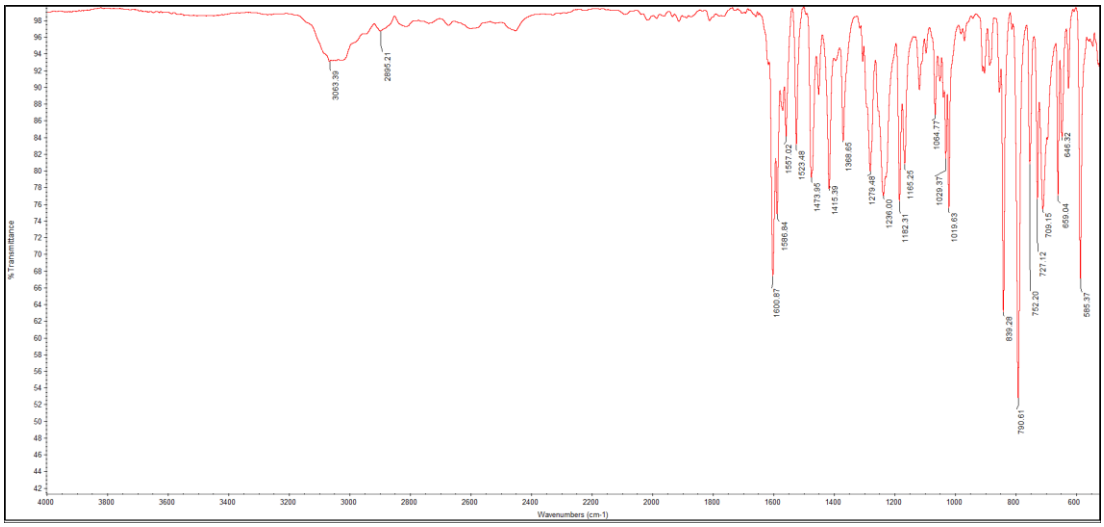


**Figure S5** The IR spectrum of compound **6**.

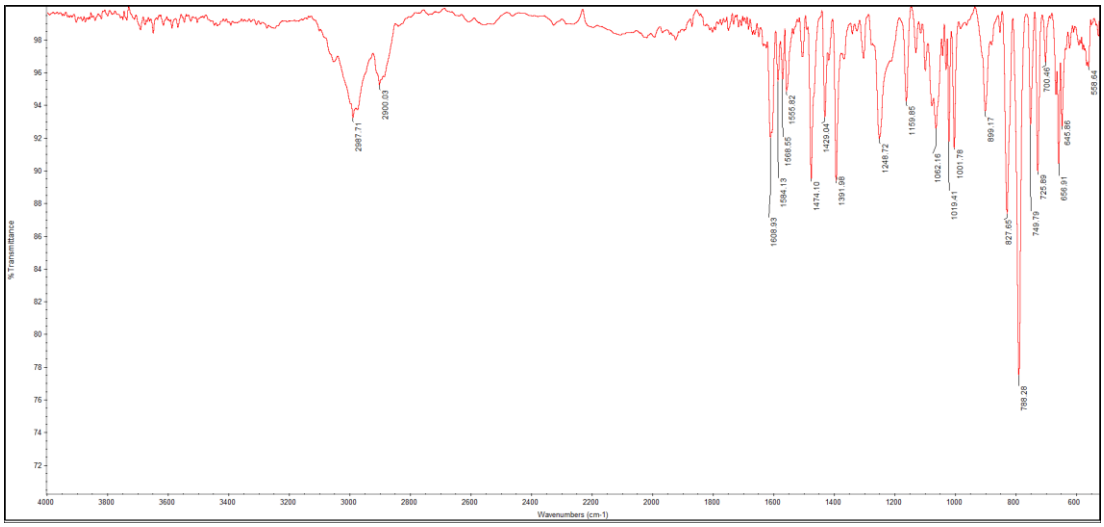


**Figure S6** The IR spectrum of compound **7**.

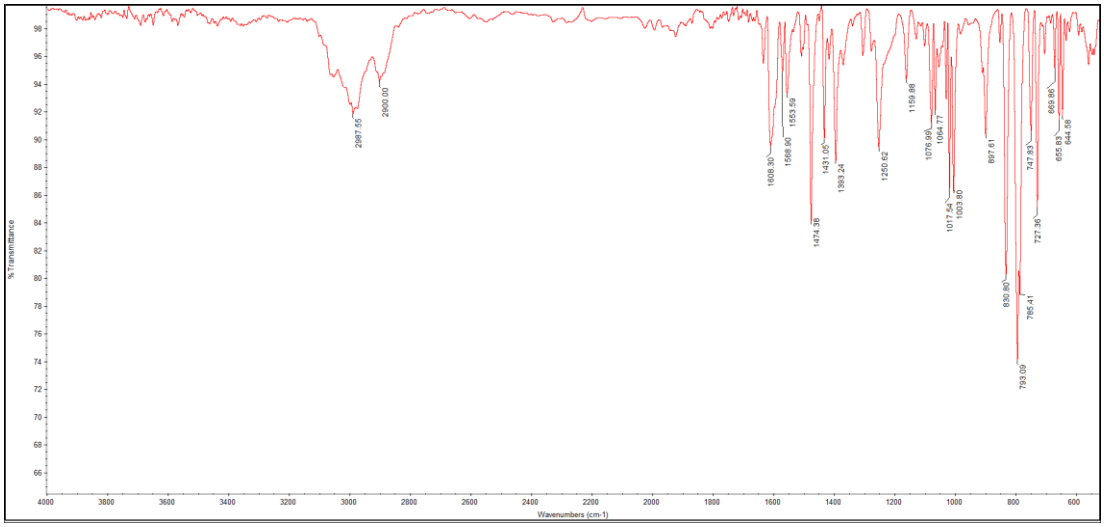


**Figure S7** The IR spectrum of compound **8**.

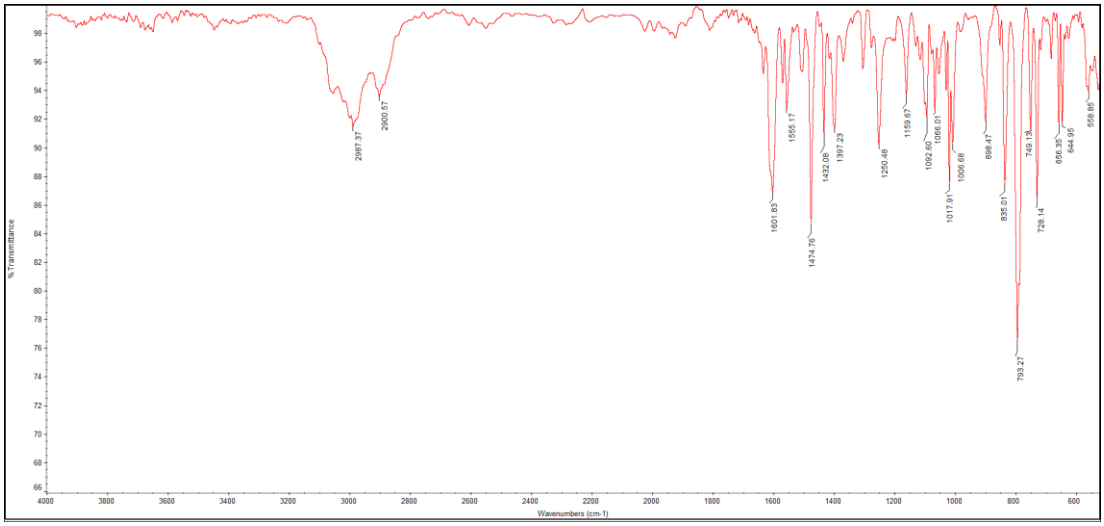


**Figure S8** The IR spectrum of compound **9**.

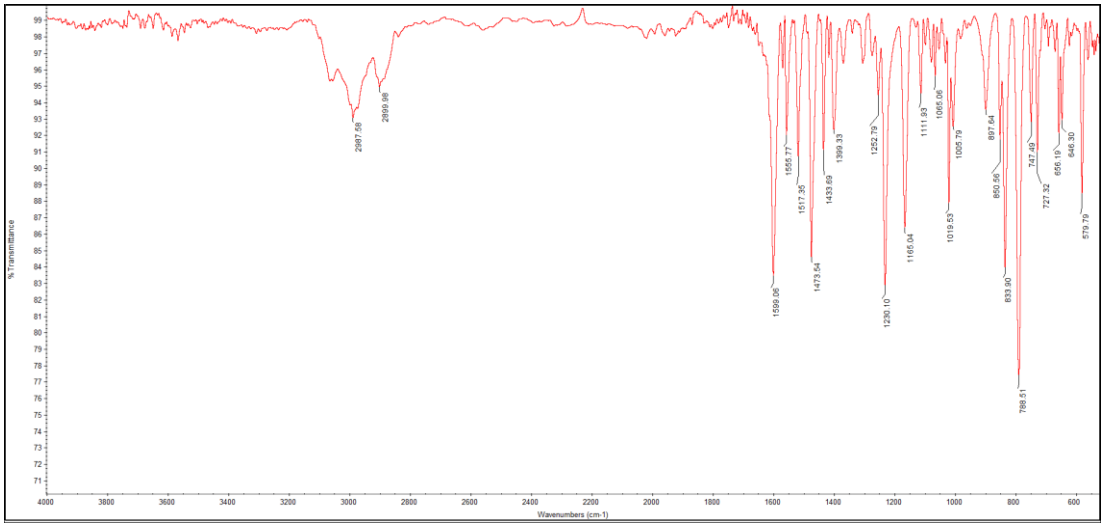


**Figure S9** The IR spectrum of compound **10**.

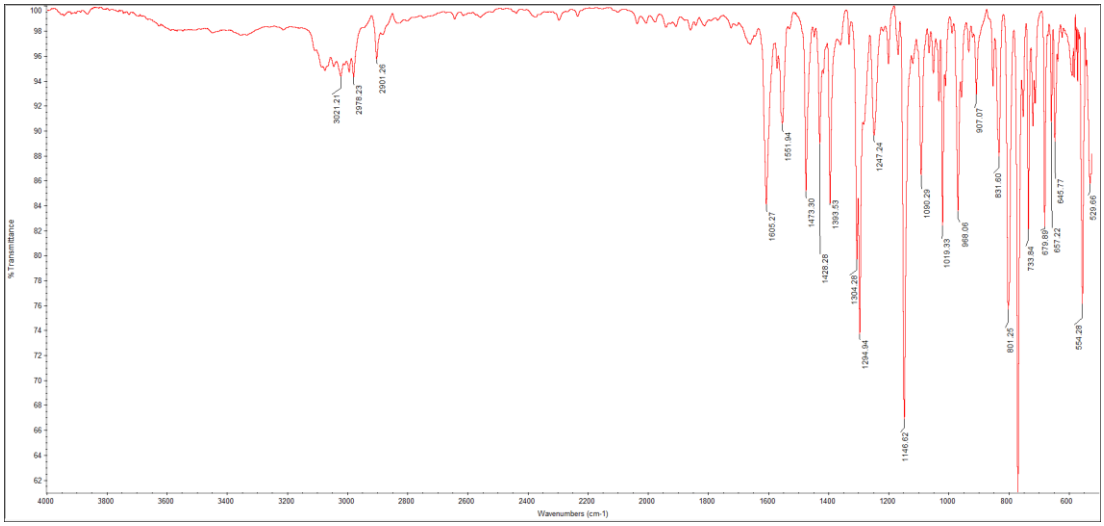


**Figure S10** The IR spectrum of compound **11**.

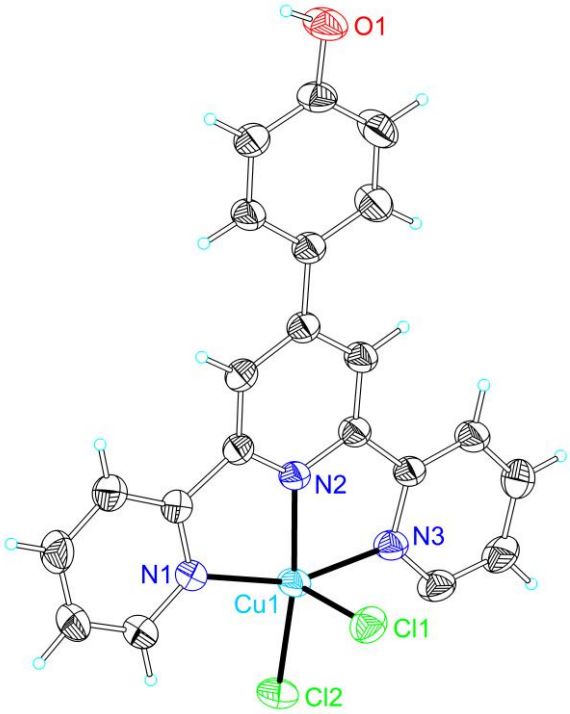


**Figure S11** Thermal ellipsoid plot, drawn at the 30% probability level, of $[CuCl_2\mathbf{L}^3]\cdot(\mathbf{3})$ with atomic numbering scheme. Selected bond lengths (Å) and angles (°): Cu(1)–N(1) 2.029(2), Cu(1)–N(2) 1.9318(18), Cu(1)–N(3) 2.030(2), Cu(1)–Cl(1) 2.5716(8), Cu(1)–Cl(2) 2.2214(8), N(2)–Cu(1)–N(3) 79.85(8), N(2)–Cu(1)–N(1) 79.00(8), N(3)–Cu(1)–N(1) 157.90(7), N(2)–Cu(1)–Cl(1) 92.08(6), N(3)–Cu(1)–Cl(1) 93.28(6), N(1)–Cu(1)–Cl(2) 93.79(6), N(2)–Cu(1)–Cl(2) 165.32(6), N(3)–Cu(1)–Cl(2) 98.78(5), N(1)–Cu(1)–Cl(2) 100.05(6), Cl(1)–Cu(1)–Cl(2) 102.60(3).

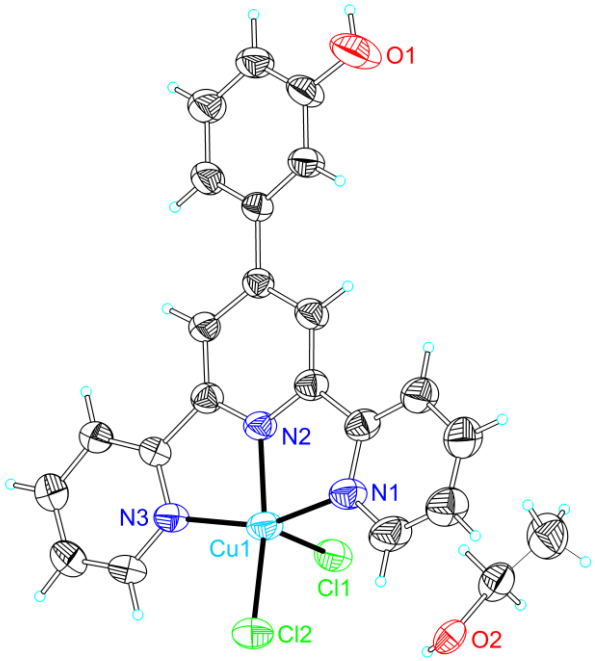


**Figure S12** Thermal ellipsoid plot, drawn at the 30% probability level, of $[CuCl_2\mathbf{L^4}]\cdot C_2H_5OH$ (**4**$\cdot C_2H_5OH$) with atomic numbering scheme. Selected bond lengths (Å) and angles (°): Cu(1)–N(1) 2.047(4), Cu(1)–N(2) 1.935(3), Cu(1)–N(3) 2.037(4), Cu(1)–Cl(1) 2.5474(15), Cu(1)–Cl(2) 2.2236(13), N(2)–Cu(1)–N(3) 79.34(14), N(2)–Cu(1)–N(1) 79.35(14), N(3)–Cu(1)–N(1) 157.01(15), N(2)–Cu(1)–Cl(1) 97.20(13), N(3)–Cu(1)–Cl(1) 93.73(12), N(1)–Cu(1)–Cl(1) 97.39(12), N(2)–Cu(1)–Cl(2) 163.28(13), N(3)–Cu(1)–Cl(2) 99.49(11), N(1)–Cu(1)–Cl(2) 98.43(11), Cl(1)–Cu(1)–Cl(2) 99.51(5).

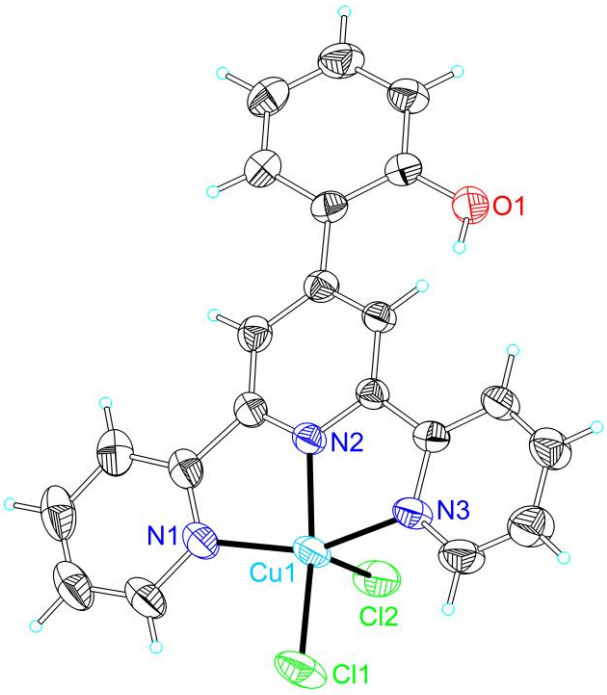


**Figure S13** Thermal ellipsoid plot, drawn at the 30% probability level, of $[CuCl_2\mathbf{L}^5]\cdot(\mathbf{5})$ with atomic numbering scheme. Selected bond lengths (Å) and angles (°): Cu(1)–N(1) 2.045(2), Cu(1)–N(2) 1.9437(16), Cu(1)–N(3) 2.0550(19), Cu(1)–Cl(1) 2.2139(7), Cu(1)–Cl(2) 2.5582(7), N(2)–Cu(1)–N(3) 79.01(7), N(2)–Cu(1)–N(1) 79.05(7), N(3)–Cu(1)–N(1) 155.79(7), N(2)–Cu(1)–Cl(1) 164.93(6), N(3)–Cu(1)–Cl(1) 98.61(5), N(1)–Cu(1)–Cl(1) 99.91(6), N(2)–Cu(1)–Cl(2) 89.94(5), N(3)–Cu(1)–Cl(2) 96.96(6), N(1)–Cu(1)–Cl(2) 93.13(5), Cl(1)–Cu(1)–Cl(2) 105.13(3).

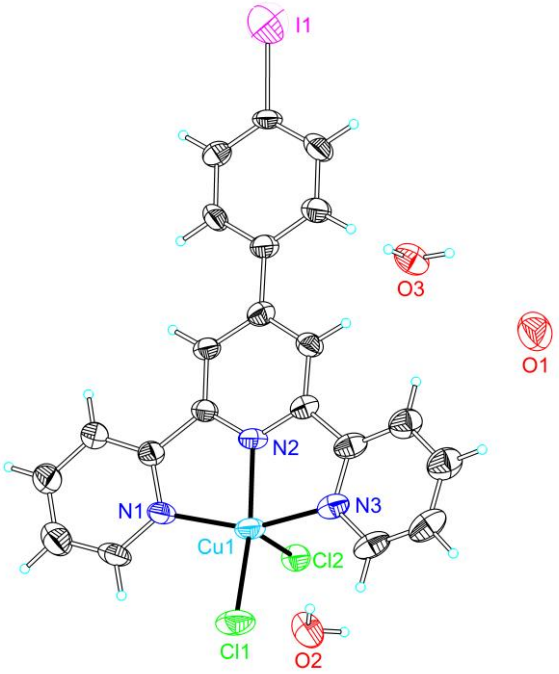


**Figure S14** Thermal ellipsoid plot, drawn at the 30% probability level, of $[CuCl_2\mathbf{L}^7]\cdot 2.5H_2O$ (**7**·$2.5H_2O$) with atomic numbering scheme. Selected bond lengths (Å) and angles (°): Cu(1)–N(1) 2.03(2), Cu(1)–N(2) 1.94(2), Cu(1)–N(3) 2.04(3), Cu(1)–Cl(1) 2.227(8), Cu(1)–Cl(2) 2.603(8), N(2)–Cu(1)–N(3) 78.9(9), N(2)–Cu(1)–N(1) 79.5(9), N(3)–Cu(1)–N(1) 156.0(9), N(2)–Cu(1)–Cl(1) 163.0(7), N(3)–Cu(1)–Cl(1) 98.8(7), N(1)–Cu(1)–Cl(1) 98.9(7), N(2)–Cu(1)–Cl(2) 95.1(7), N(3)–Cu(1)–Cl(2) 96.9(7), N(1)–Cu(1)–Cl(2) 95.2(7), Cl(1)–Cu(1)–Cl(2) 101.8(3).

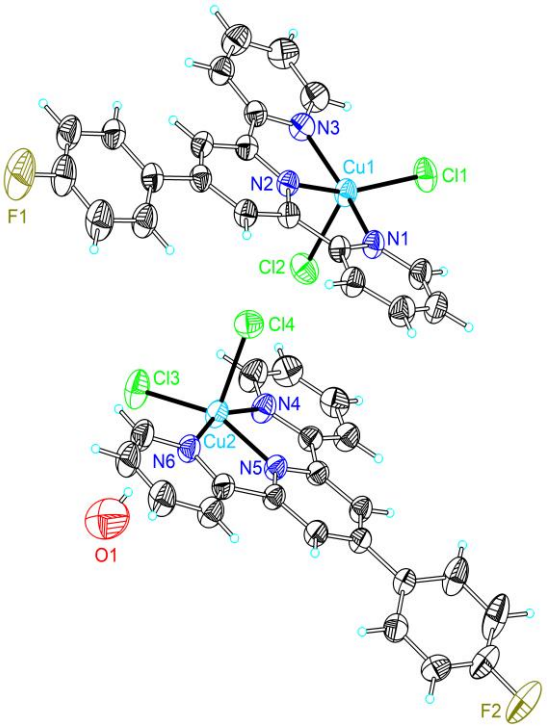


**Figure S15** Thermal ellipsoid plot, drawn at the 30% probability level, of $[CuCl_2\mathbf{L}^{10}]_2 \cdot H_2O$ (**10**·0.5$H_2O$) with atomic numbering scheme. Selected bond lengths (Å) and angles (°): Cu(1)–N(1) 2.0475(17), Cu(1)–N(2) 1.9488(17), Cu(1)–N(3) 2.0415(18), Cu(1)–Cl(1) 2.2467(6), Cu(1)–Cl(2) 2.4919(6), Cu(2)–N(5) 1.9579(16), Cu(2)–N(4) 2.0359(19), Cu(2)–N(6) 2.0382(18), Cu(2)–Cl(3) 2.2543(6), Cu(2)–Cl(4) 2.4396(6), N(2)–Cu(1)–N(3) 79.03(7), N(2)–Cu(1)–N(1) 78.76(7), N(3)–Cu(1)–N(1) 155.85(7), N(2)–Cu(1)–Cl(1) 157.19(5), N(3)–Cu(1)–Cl(1) 97.98(6), N(1)–Cu(1)–Cl(1) 98.81(5), N(2)–Cu(1)–Cl(2) 99.94(5), N(3)–Cu(1)–Cl(2) 94.18(5), N(1)–Cu(1)–Cl(2) 98.85(5), Cl(1)–Cu(1)–Cl(2) 102.84(2), N(5)–Cu(2)–N(4) 78.57(7), N(5)–Cu(2)–N(6) 79.07(7), N(4)–Cu(2)–N(6) 156.64(7), N(5)–Cu(2)–Cl(3) 153.85(5), N(4)–Cu(2)–Cl(3) 97.47(5), N(6)–Cu(2)–Cl(3) 99.61(5), N(5)–Cu(2)–Cl(4) 102.08(5), N(4)–Cu(2)–Cl(4) 96.09(5), N(6)–Cu(2)–Cl(4) 95.11(5), Cl(3)–Cu(2)–Cl(4) 104.04(3).

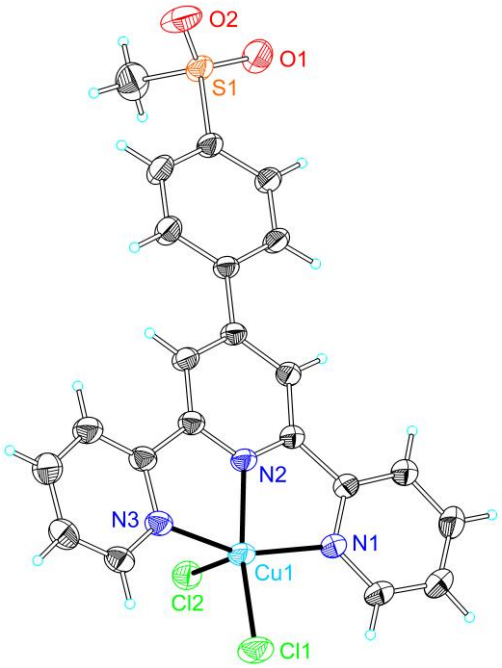


**Figure S16** Thermal ellipsoid plot, drawn at the 30% probability level, of [$CuCl_2$**L**$^{11}$] (**11**) with atomic numbering scheme. Selected bond lengths (Å) and angles (°): Cu(1)–N(1) 2.0400(16), Cu(1)–N(2) 1.9415(14), Cu(1)–N(3) 2.0417(15), Cu(1)–Cl(1) 2.2134(5), Cu(1)–Cl(2) 2.5528(5), N(2)–Cu(1)–N(3) 79.41(6), N(2)–Cu(1)–N(1) 79.45(6), N(3)–Cu(1)–N(1) 156.73(6), N(2)–Cu(1)–Cl(1) 161.33(5), N(3)–Cu(1)–Cl(1) 98.39(4), N(1)–Cu(1)–Cl(1) 98.51(4), N(2)–Cu(1)–Cl(2) 89.75(5), N(3)–Cu(1)–Cl(2) 97.08(5), N(1)–Cu(1)–Cl(2) 92.44(5), Cl(1)–Cu(1)–Cl(2) 108.90(2).

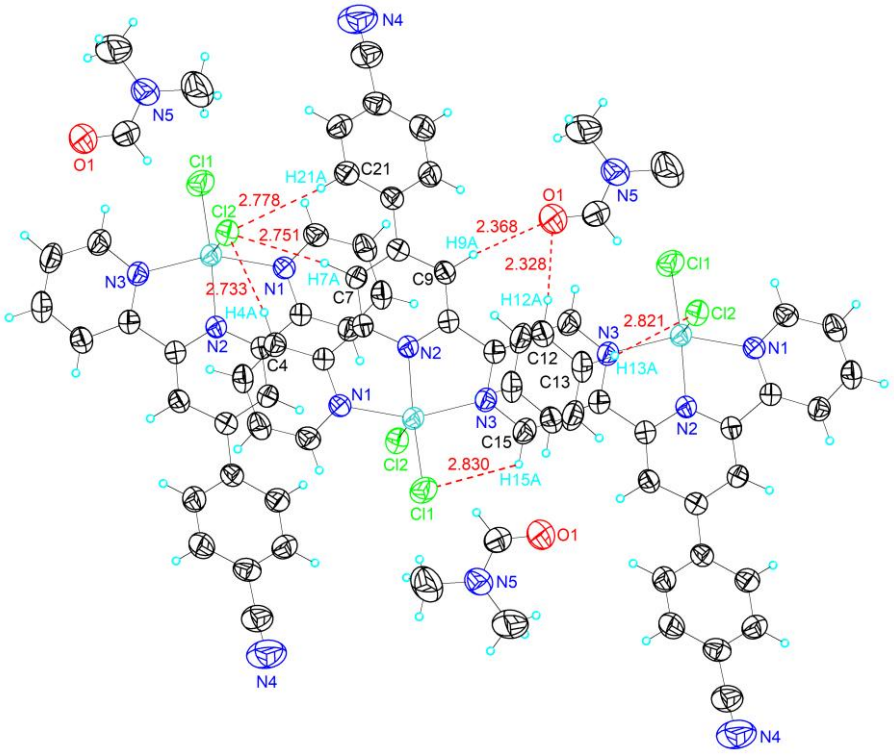


**Figure S17** The packing diagram of [$CuCl_2\mathbf{L}^2$]·DMF (**2**·DMF) with atomic numbering scheme, the intermolecular and intramolecular hydrogen bonds with lengths have been marked.

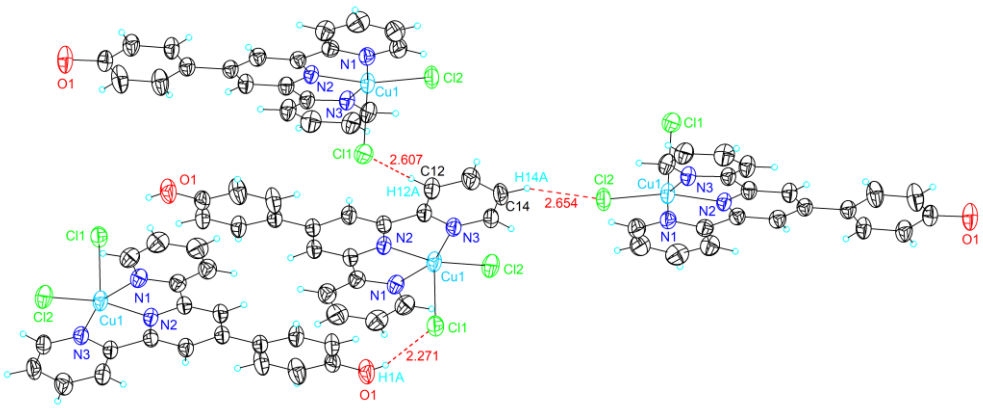


**Figure S18** The packing diagram of [$CuCl_2\mathbf{L}^3$]·(**3**) with atomic numbering scheme, the intermolecular and intramolecular hydrogen bonds with lengths have been marked.

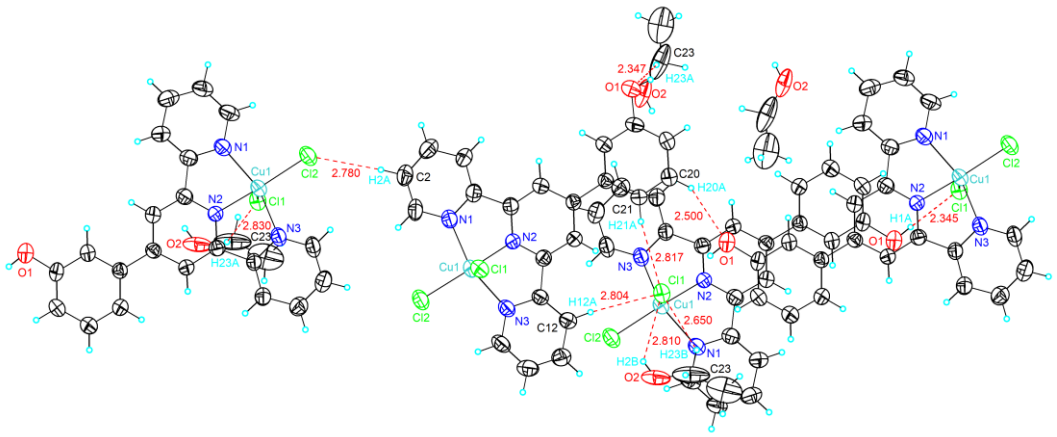


**Figure S19** The packing diagram of $[CuCl_2\mathbf{L}^4]\cdot C_2H_5OH$ (**4**·$C_2H_5OH$) with atomic numbering scheme, the intermolecular and intramolecular hydrogen bonds with lengths have been marked.

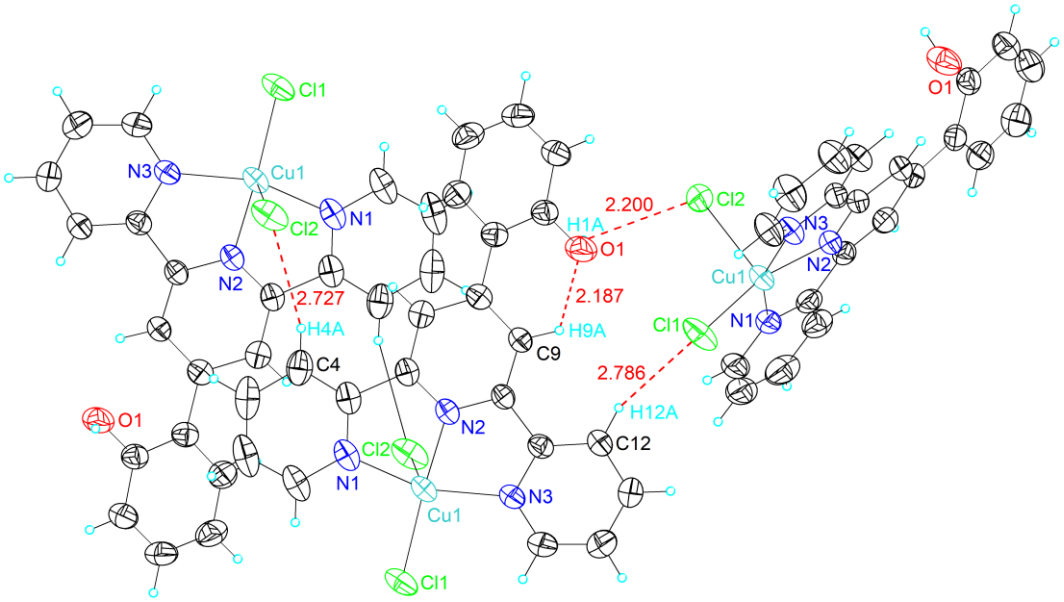


**Figure S20** The packing diagram of $[CuCl_2\mathbf{L}^5]\cdot$(**5**) with atomic numbering scheme, the intermolecular and intramolecular hydrogen bonds with lengths have been marked.

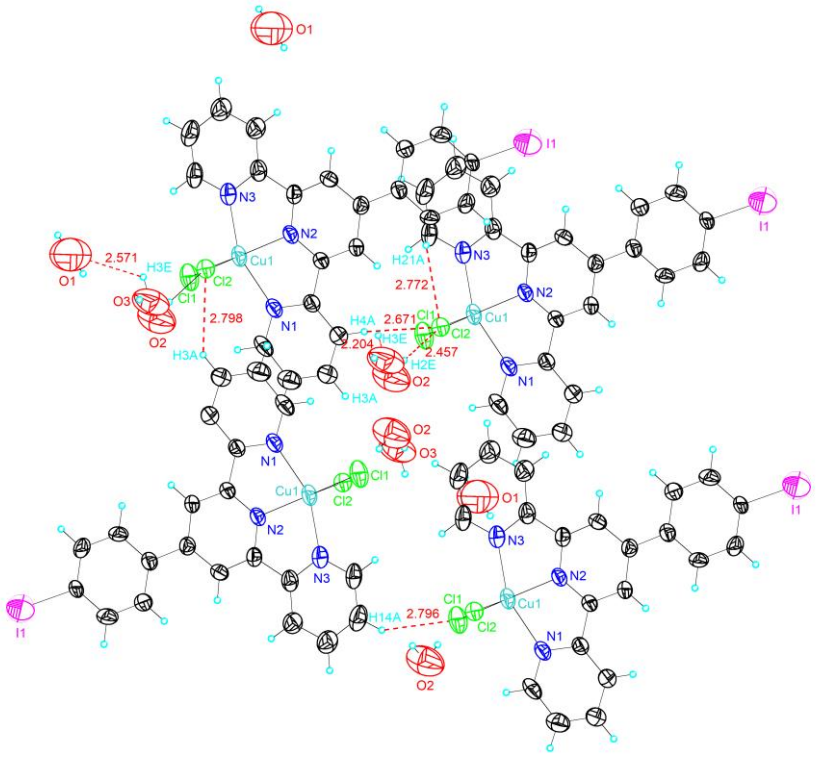


**Figure S21** The packing diagram of $[CuCl_2\mathbf{L}^7]\cdot 2.5H_2O$ (**7**·$2.5H_2O$) with atomic numbering scheme, the intermolecular and intramolecular hydrogen bonds with lengths have been marked.

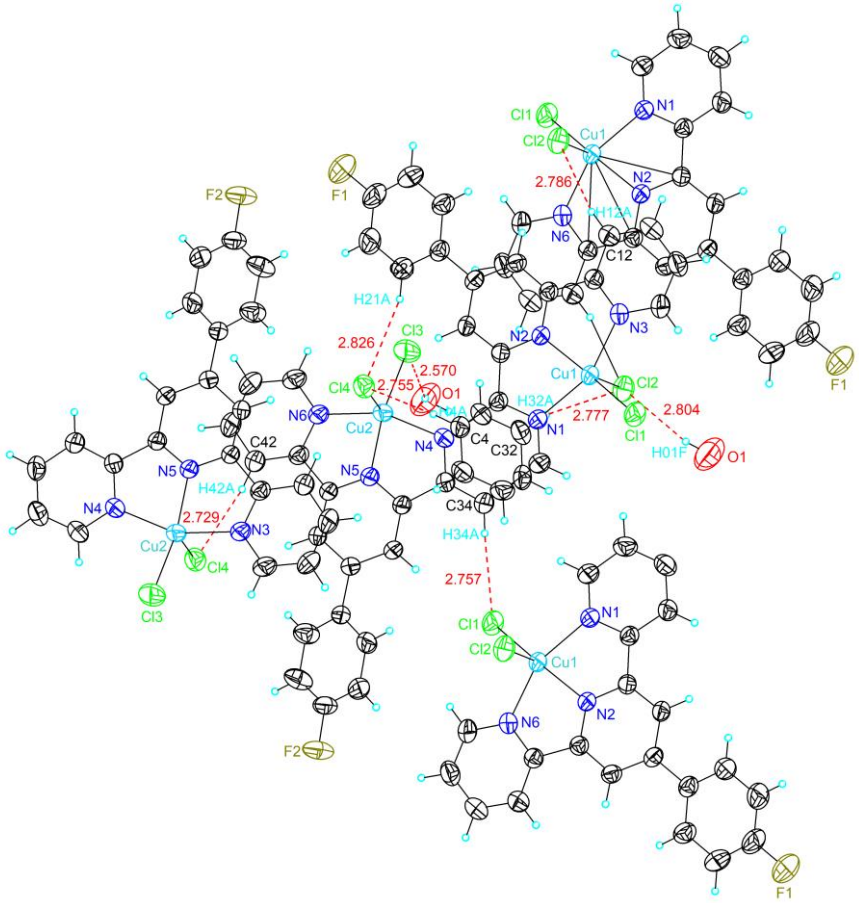


**Figure S22** The packing diagram of $[CuCl_2\mathbf{L}^{10}]_2{\cdot}H_2O$ (**10**·0.5$H_2O$) with atomic numbering scheme, the intermolecular and intramolecular hydrogen bonds with lengths have been marked.

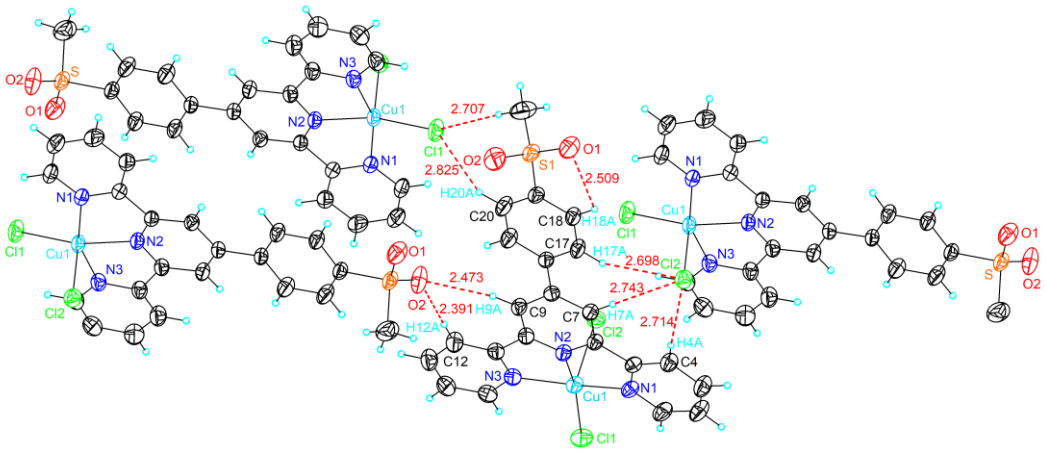


**Figure S23** The packing diagram of $[CuCl_2\mathbf{L}^{11}]$ (**11**) with atomic numbering scheme, the intermolecular and intramolecular hydrogen bonds with lengths have been marked.

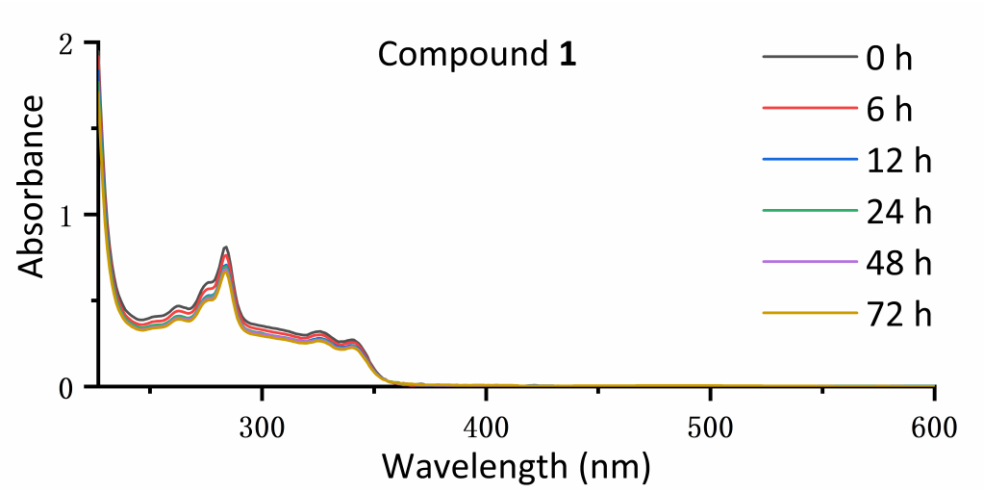


**Figure S24** UV−vis spectra of compounds **1** in Tris-HCl buffer (pH 7.2) at 25 °C for a period of 72 h.

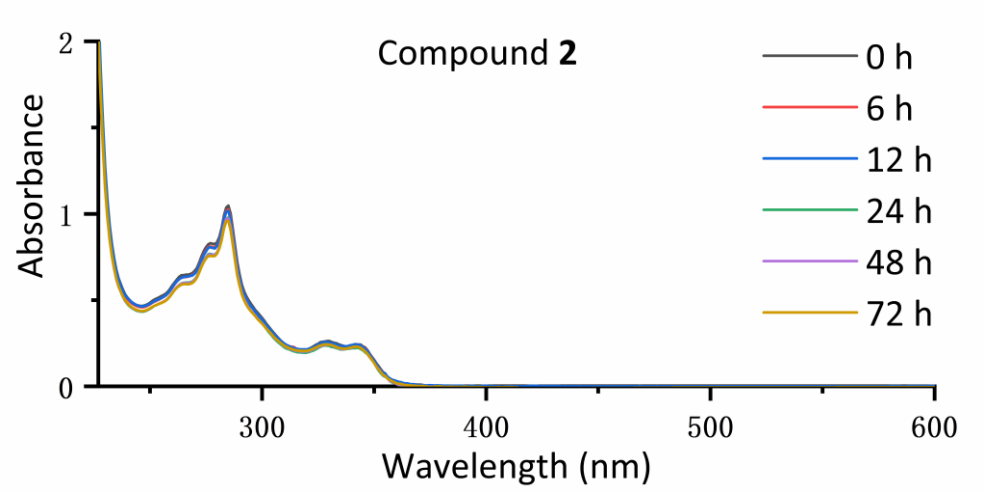


**Figure S25** UV−vis spectra of compounds **2** in Tris-HCl buffer (pH 7.2) at 25 °C for a period of 72 h.

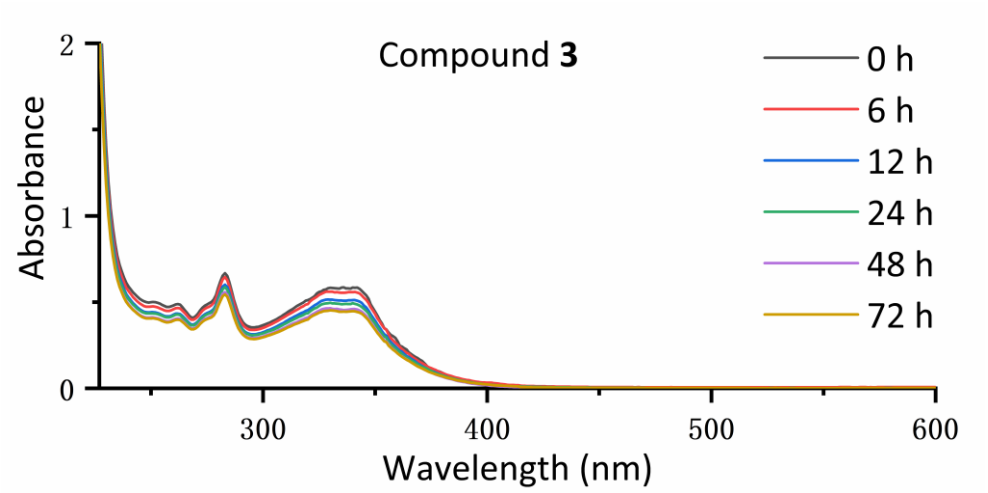


**Figure S26** UV−vis spectra of compounds **3** in Tris-HCl buffer (pH 7.2) at 25 °C for a period of 72 h.

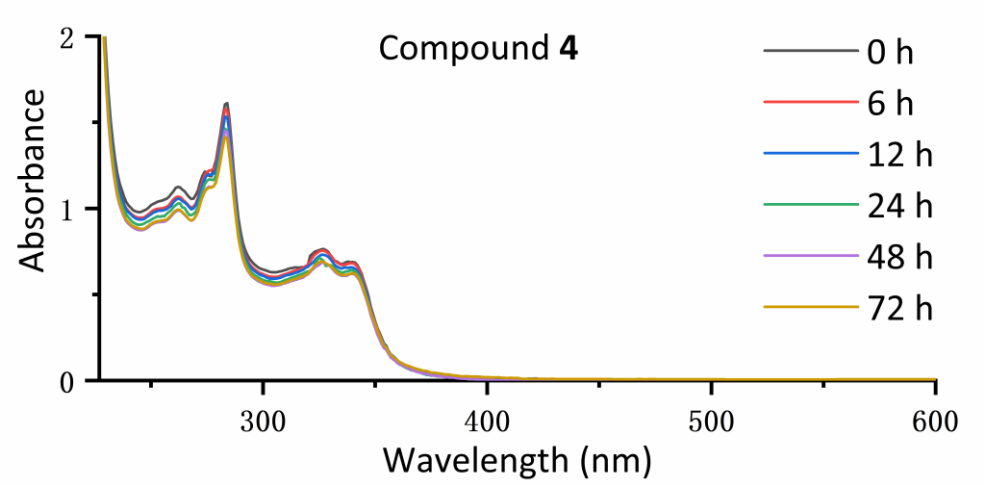


**Figure S27** UV−vis spectra of compounds **4** in Tris-HCl buffer (pH 7.2) at 25 °C for a period of 72 h.

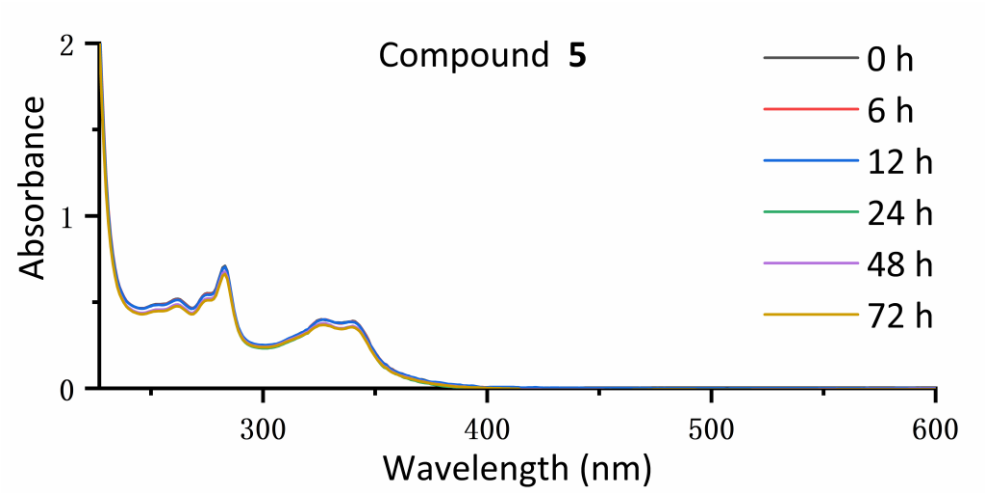


**Figure S28** UV−vis spectra of compounds **5** in Tris-HCl buffer (pH 7.2) at 25 °C for a period of 72 h.

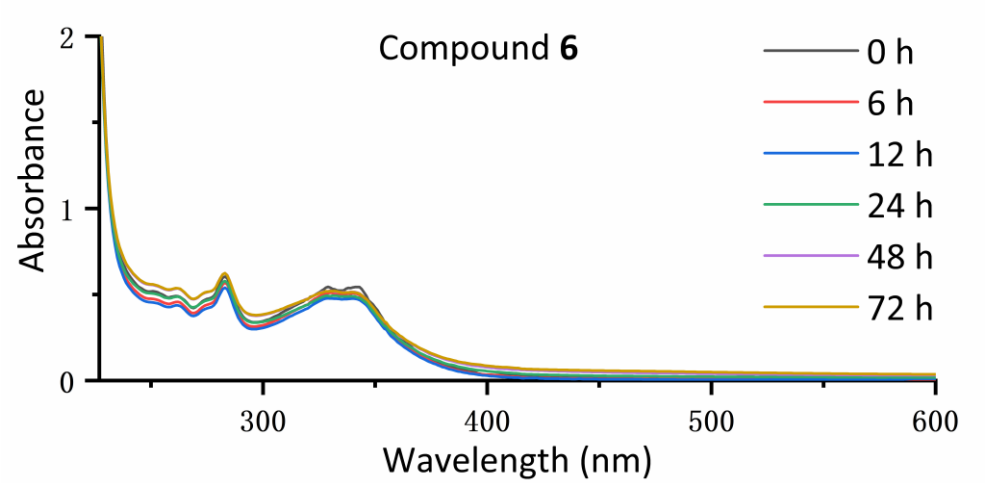


**Figure S29** UV−vis spectra of compounds **6** in Tris-HCl buffer (pH 7.2) at 25 °C for a period of 72 h.

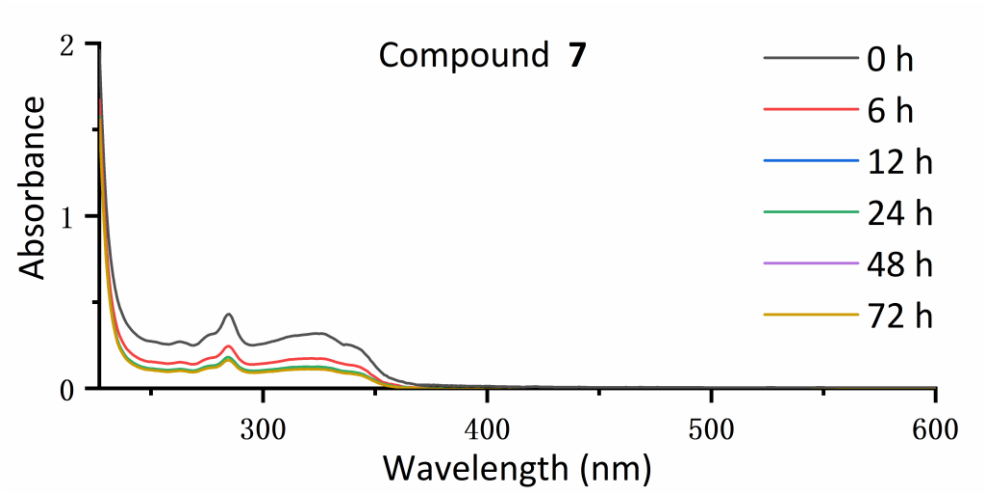


**Figure S30** UV−vis spectra of compounds **7** in Tris-HCl buffer (pH 7.2) at 25 °C for a period of 72 h.

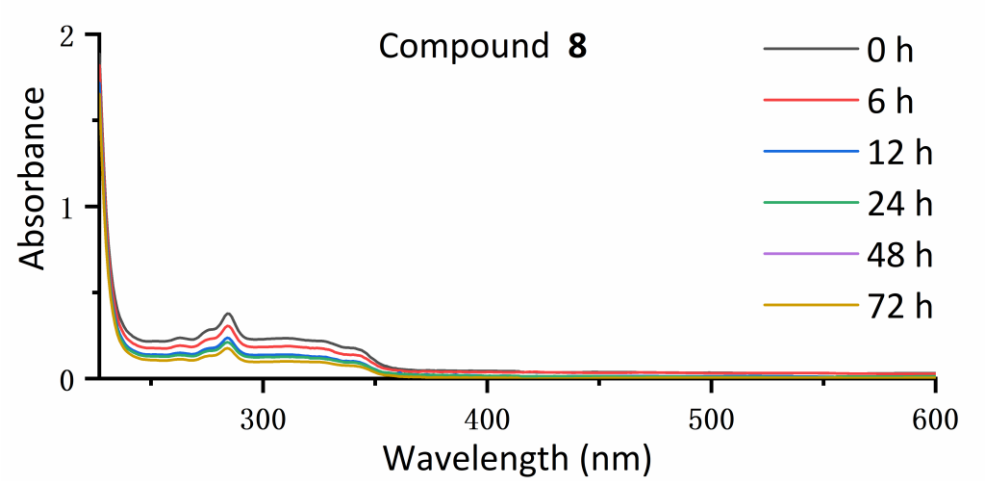


**Figure S31** UV−vis spectra of compounds **8** in Tris-HCl buffer (pH 7.2) at 25 °C for a period of 72 h.

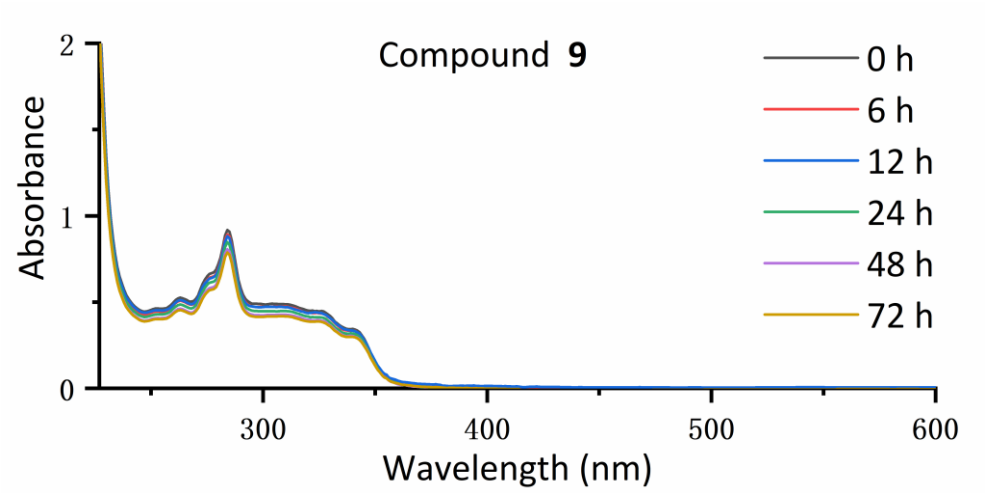


**Figure S32** UV−vis spectra of compounds **9** in Tris-HCl buffer (pH 7.2) at 25 °C for a period of 72 h.

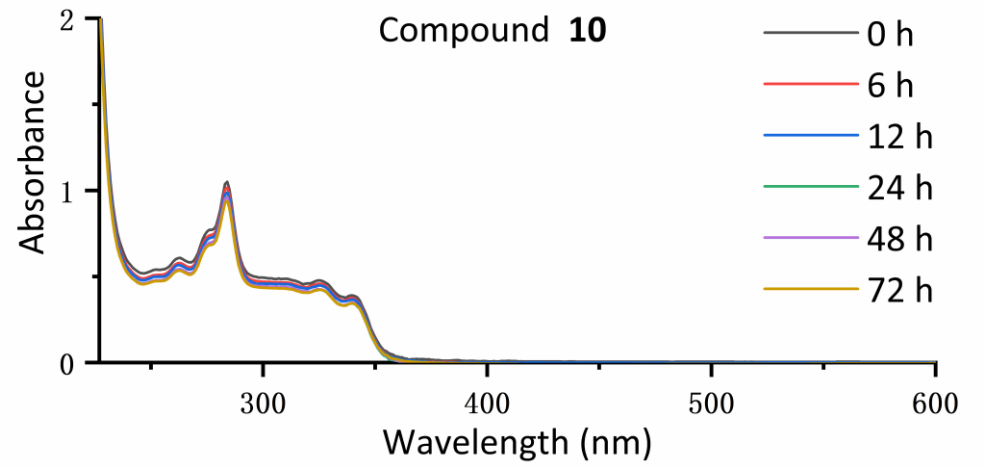


**Figure S33** UV−vis spectra of compounds **10** in Tris-HCl buffer (pH 7.2) at 25 °C for a period of 72 h.

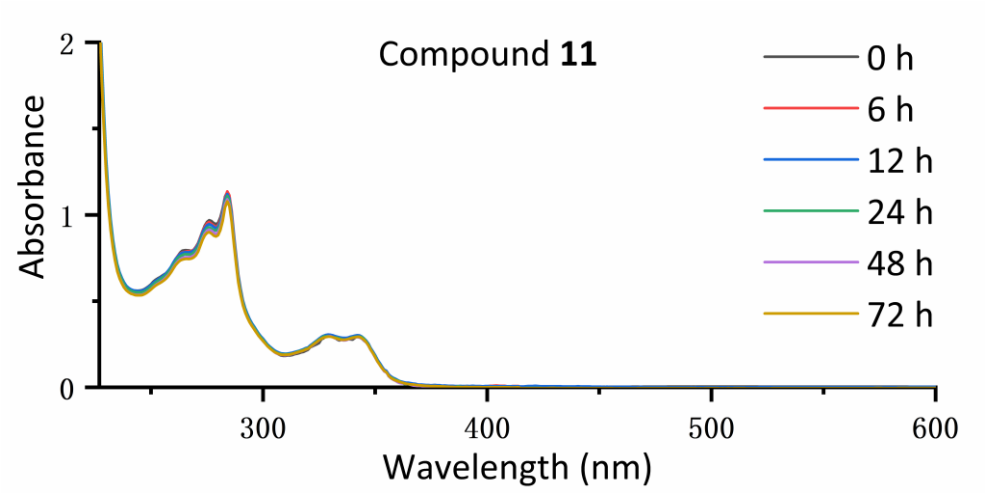


**Figure S34** UV−vis spectra of compounds **11** in Tris-HCl buffer (pH 7.2) at 25 °C for a period of 72 h.

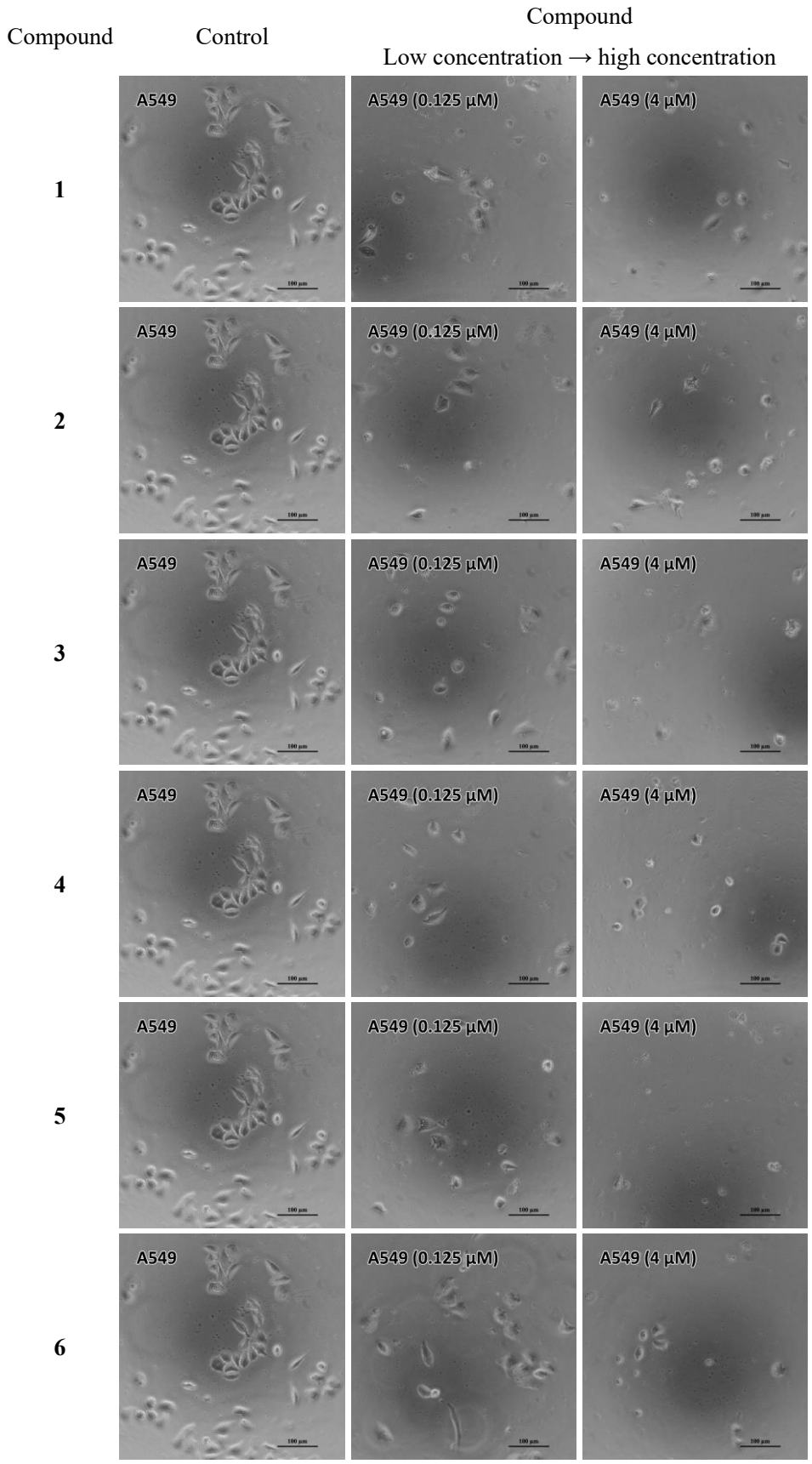


**Figure S35** The microscopic images of A549 cells treated with increased concentrations of compounds **1**–**6**.

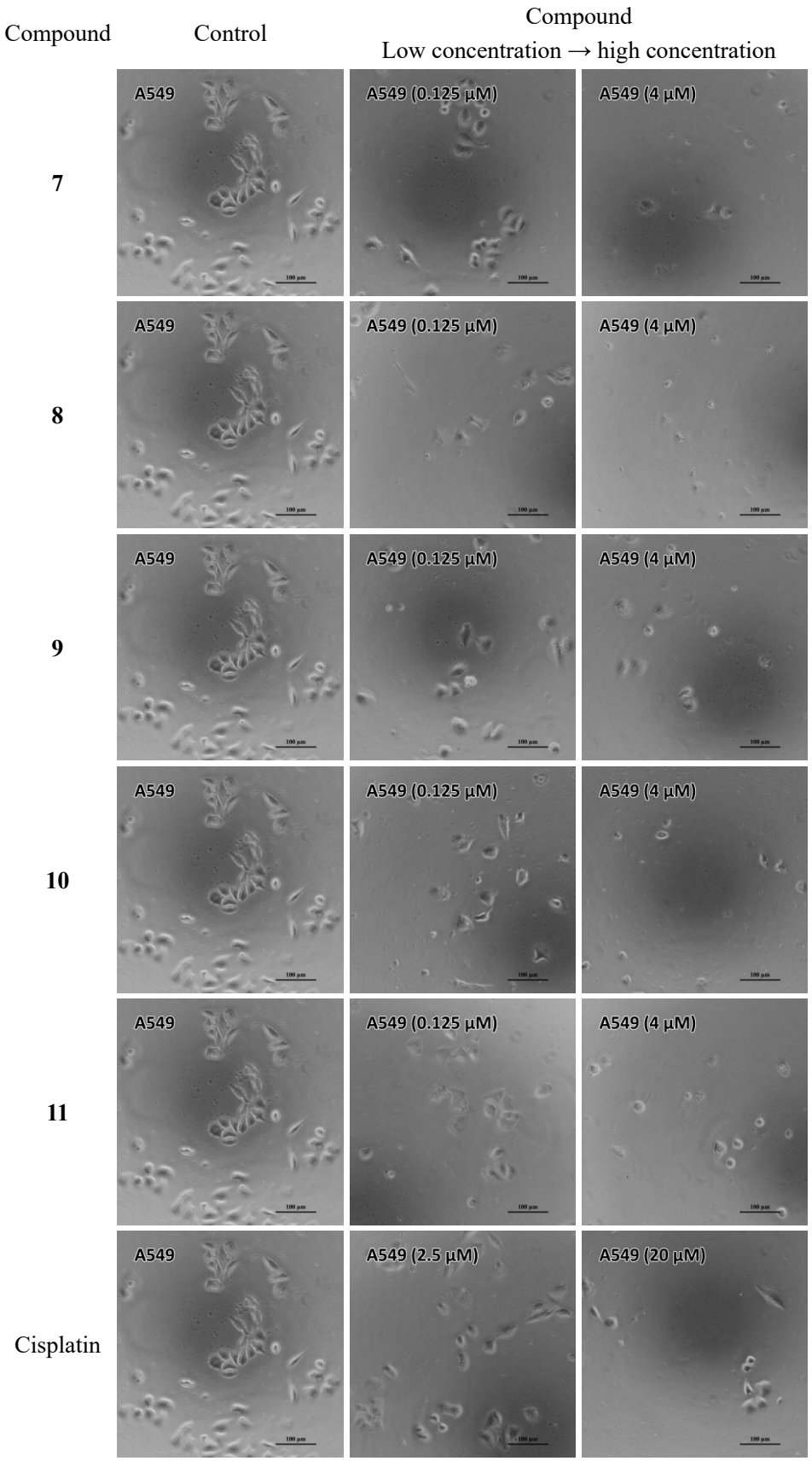


**Figure S36** The microscopic images of A549 cells treated with increased concentrations of compounds **7**–**11** and cisplatin.

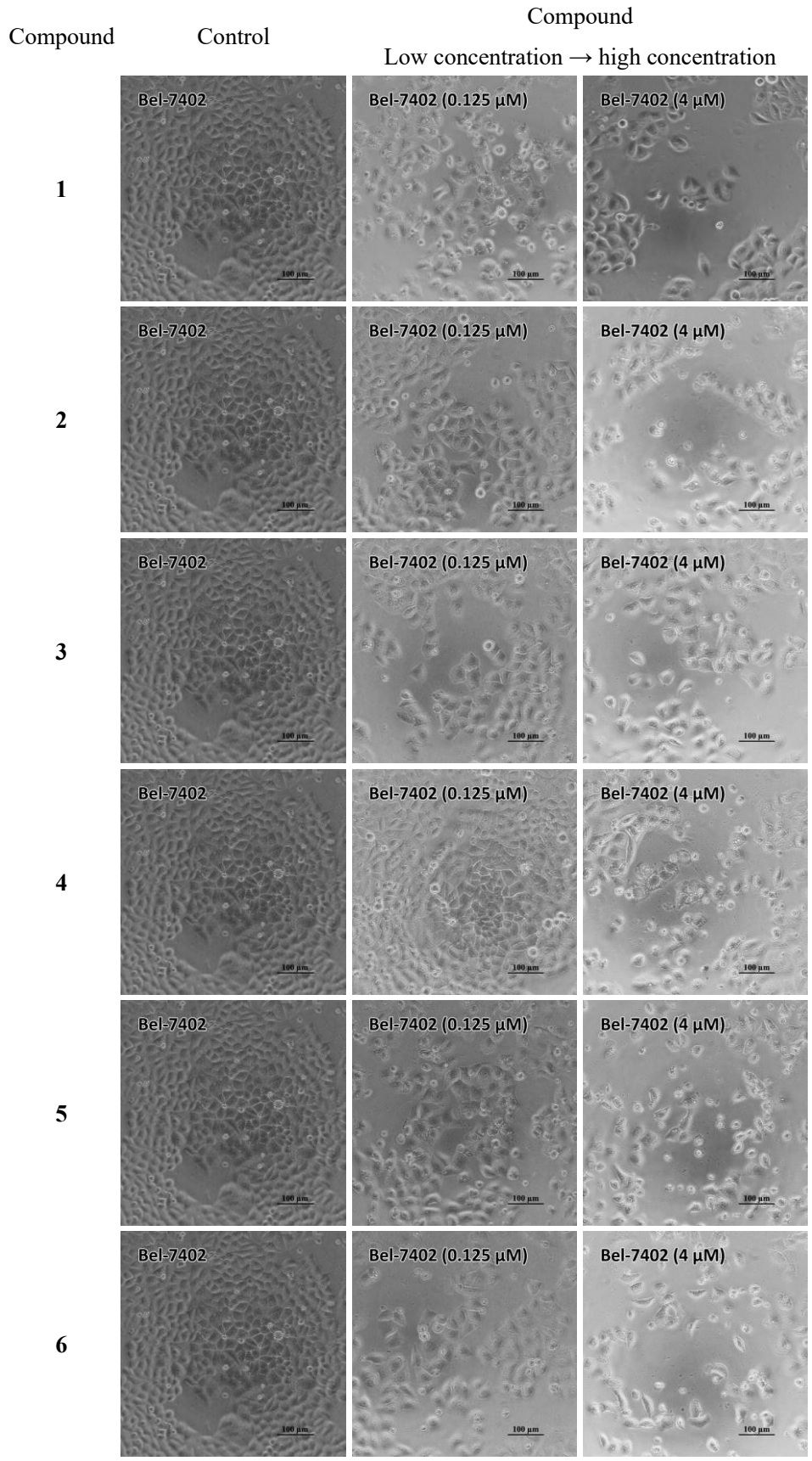


**Figure S37** The microscopic images of Bel-7402 cells treated with increased concentrations of compounds **1**–**6**.

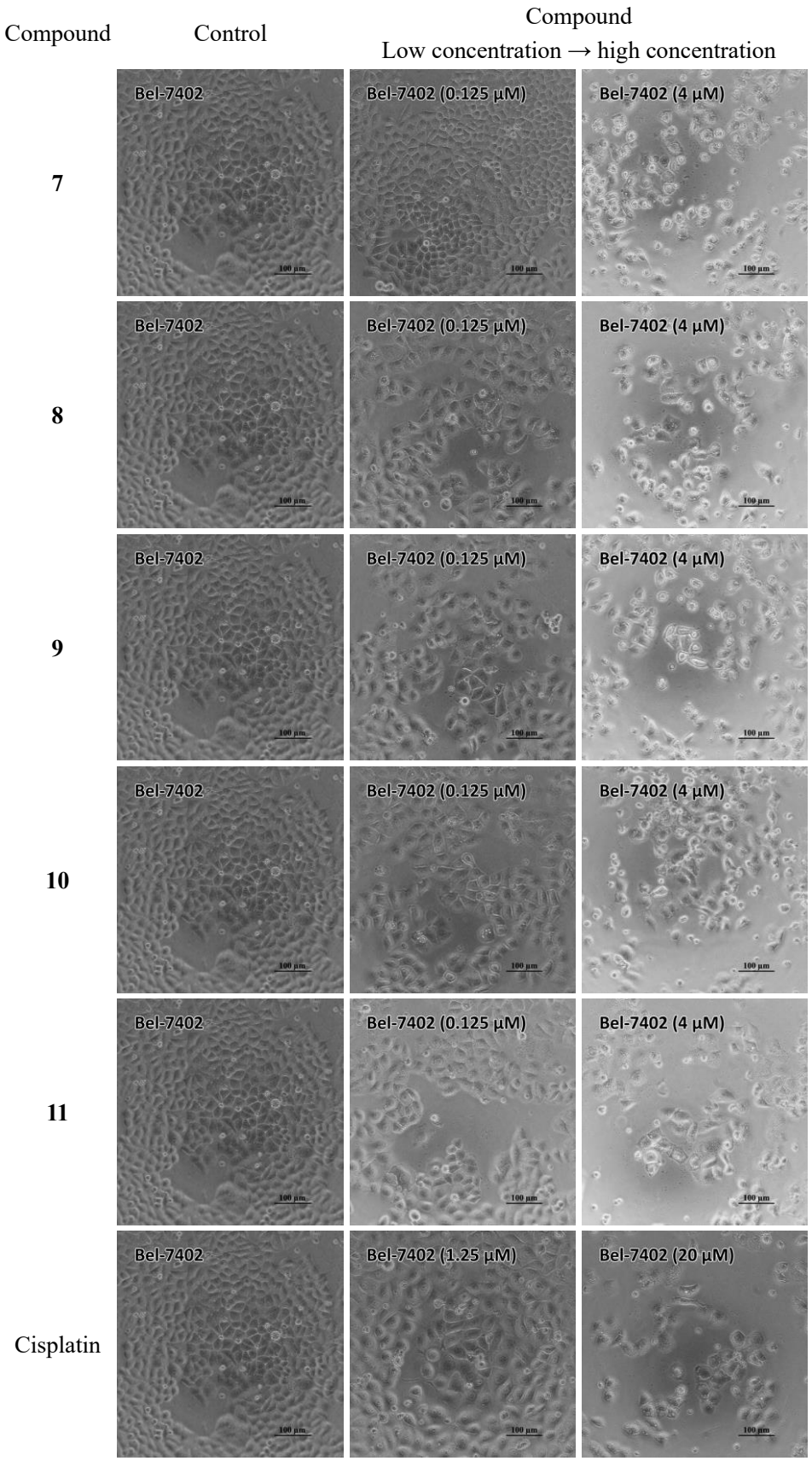


**Figure S38** The microscopic images of Bel-7402 cells treated with increased concentrations of compounds **7**–**11** and cisplatin.

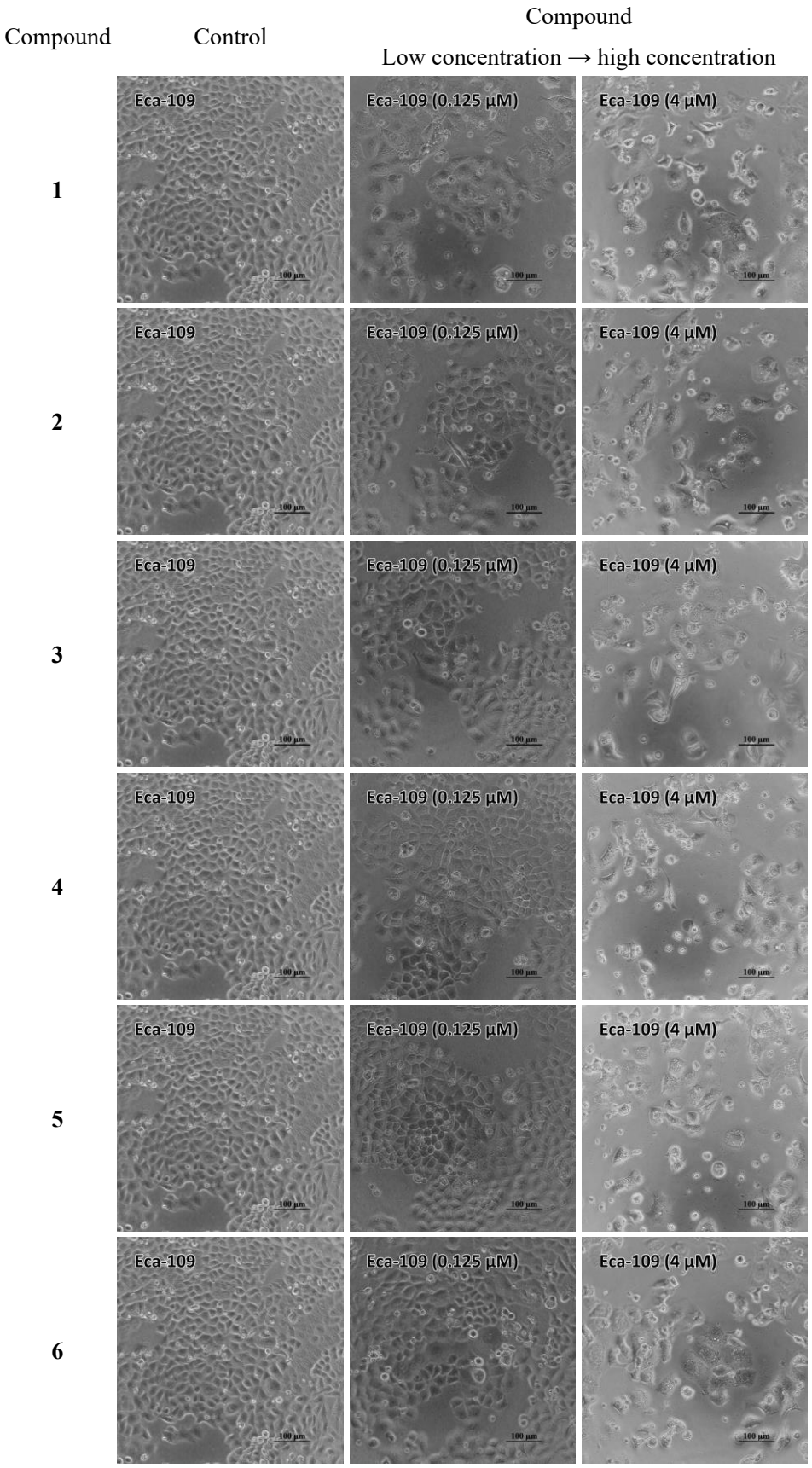


**Figure S39** The microscopic images of Eca-109 cells treated with increased concentrations of compounds **1**–**6**.

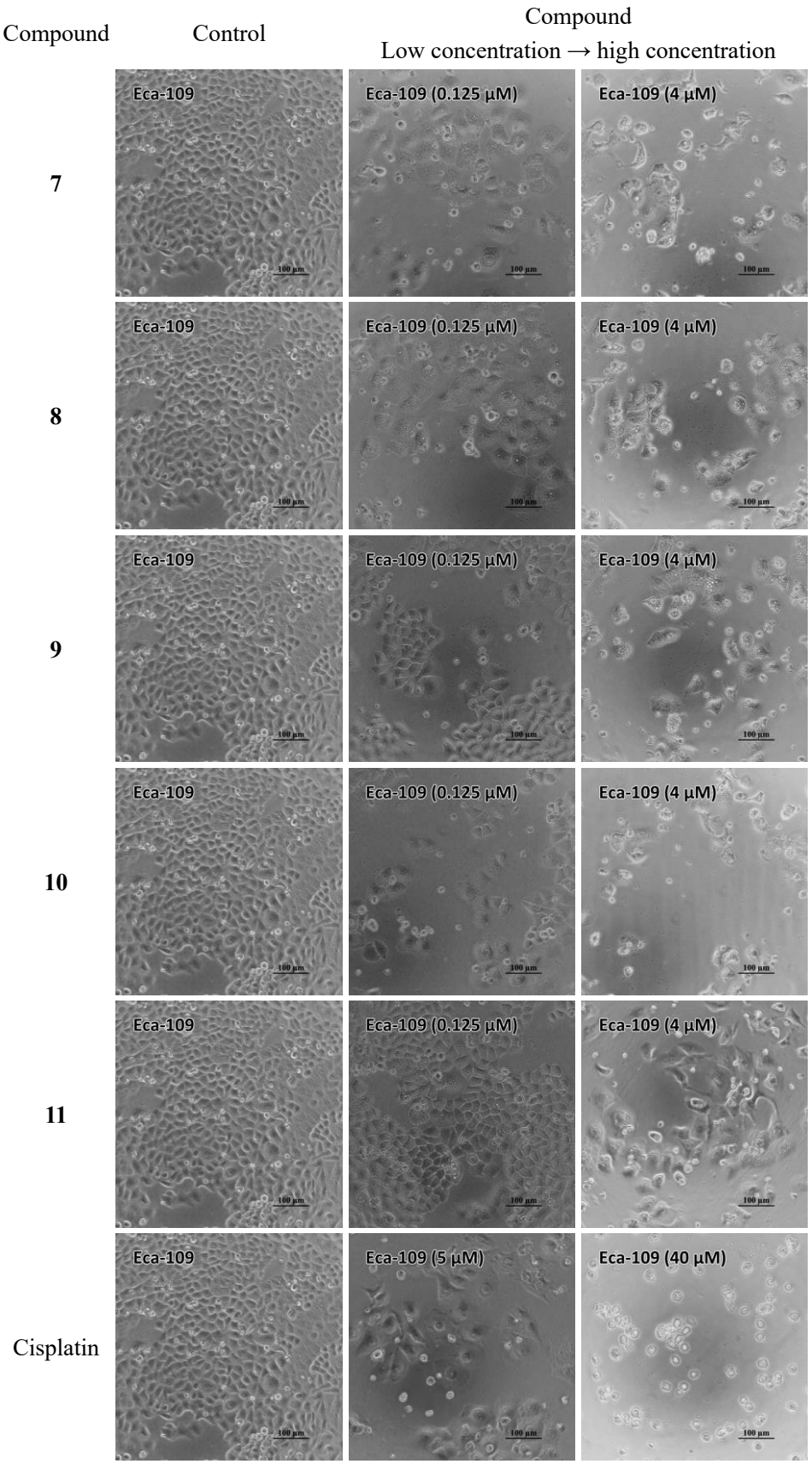


**Figure S40** The microscopic images of Eca-109 cells treated with increased concentrations of compounds **7**–**11** and cisplatin.

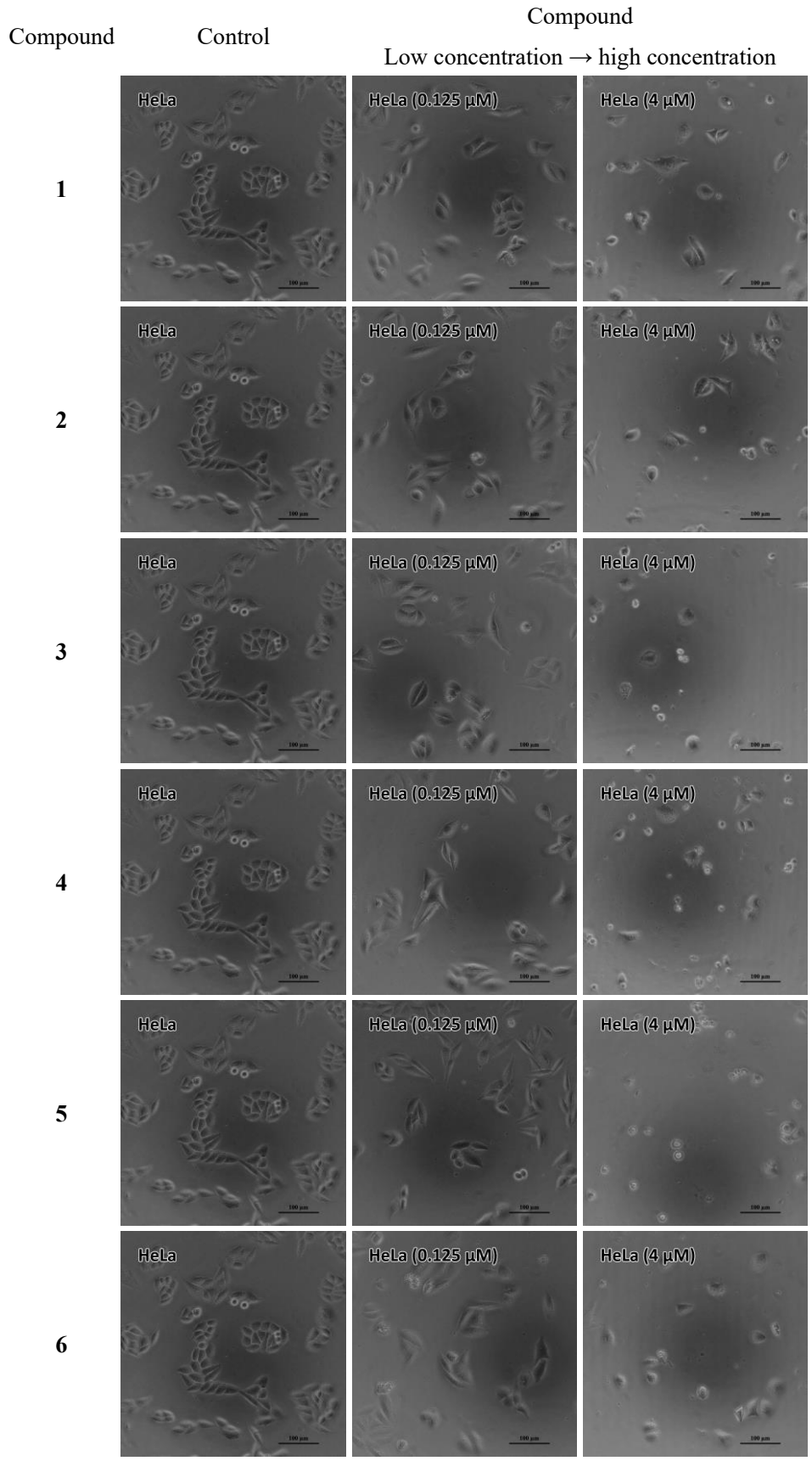


**Figure S41** The microscopic images of HeLa cells treated with increased concentrations of compounds **1**–**6**.

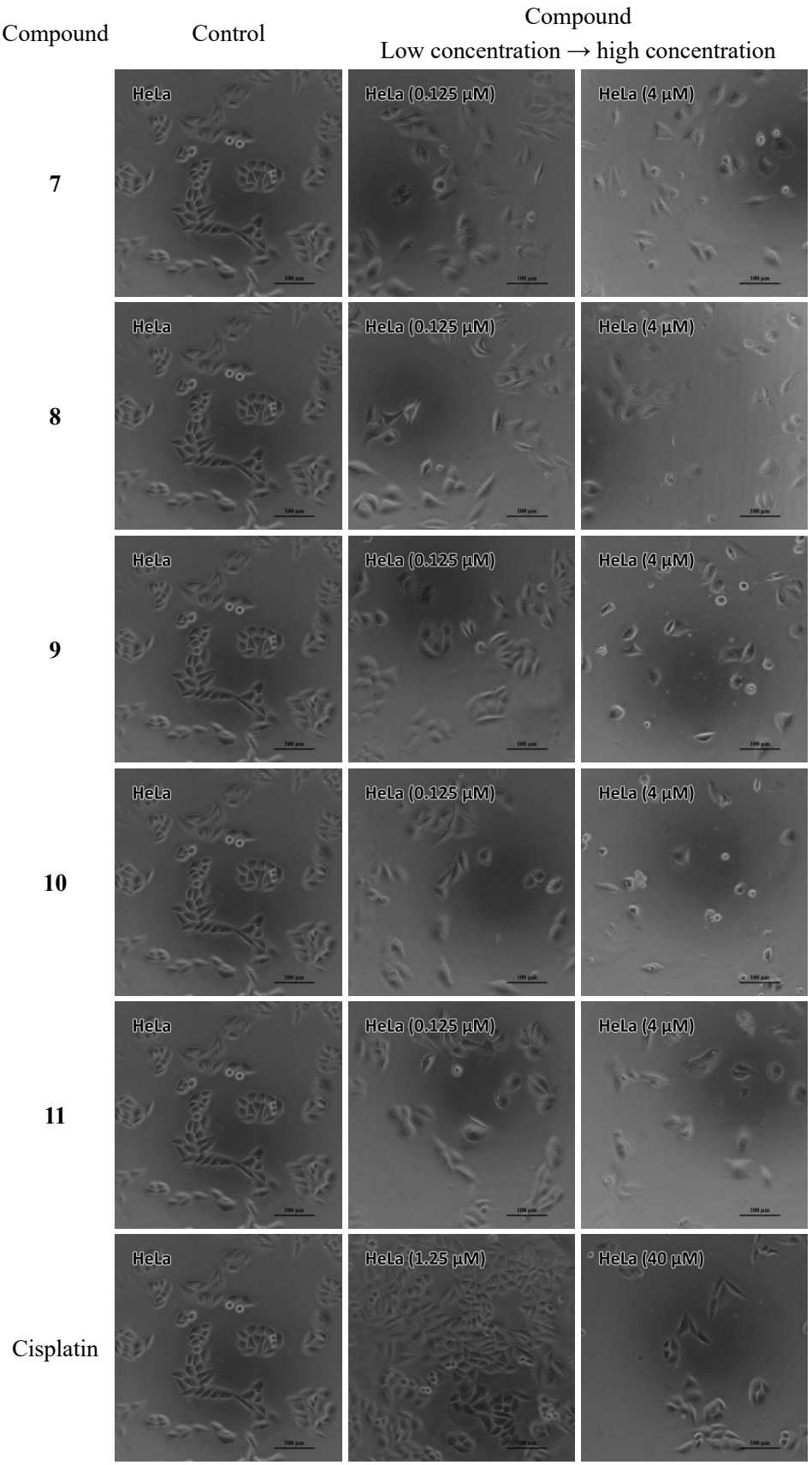


**Figure S42** The microscopic images of HeLa cells treated with increased concentrations of compounds **7**–**11** and cisplatin.

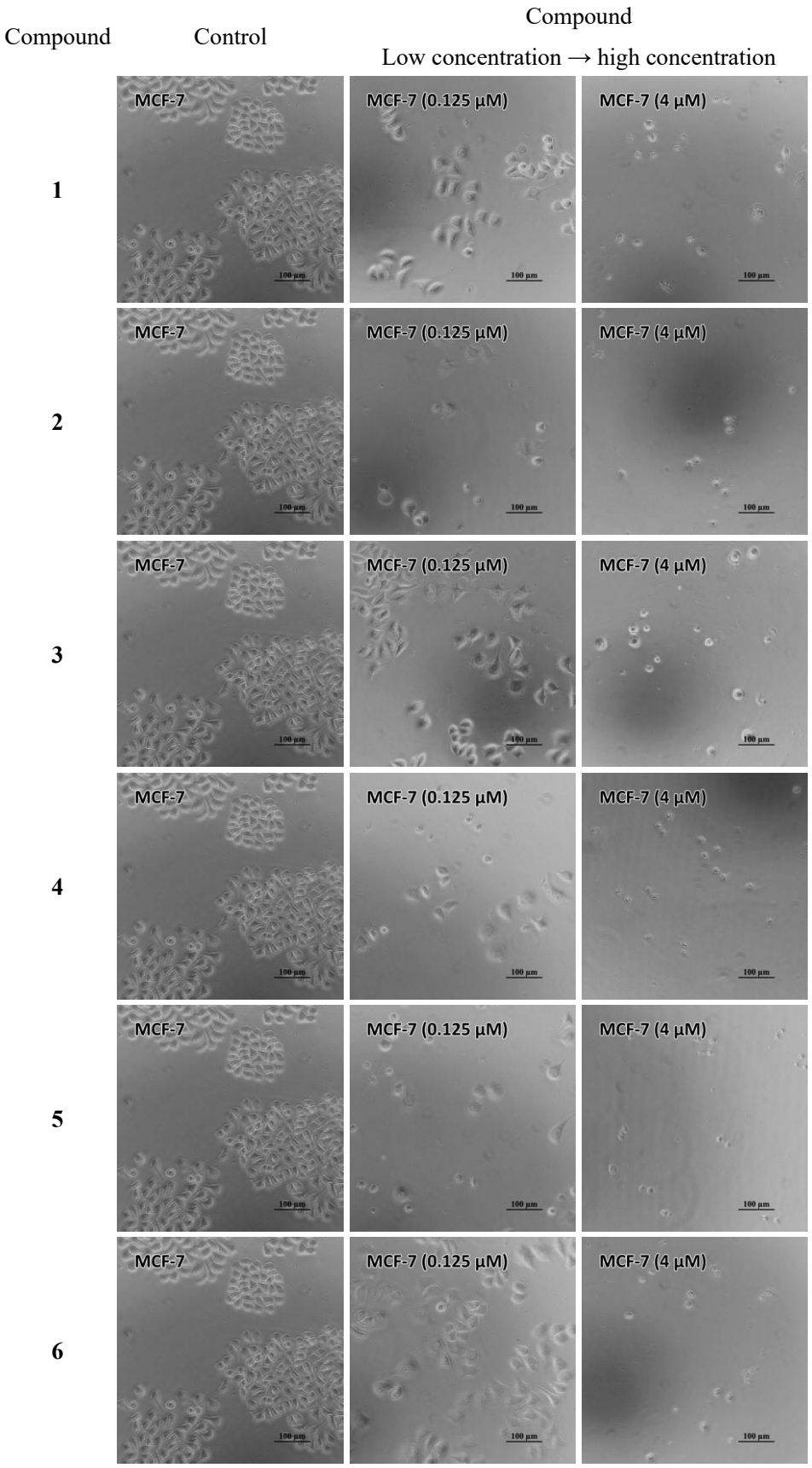


**Figure S43** The microscopic images of MCF-7 cells treated with increased concentrations of compounds **1**–**6**.

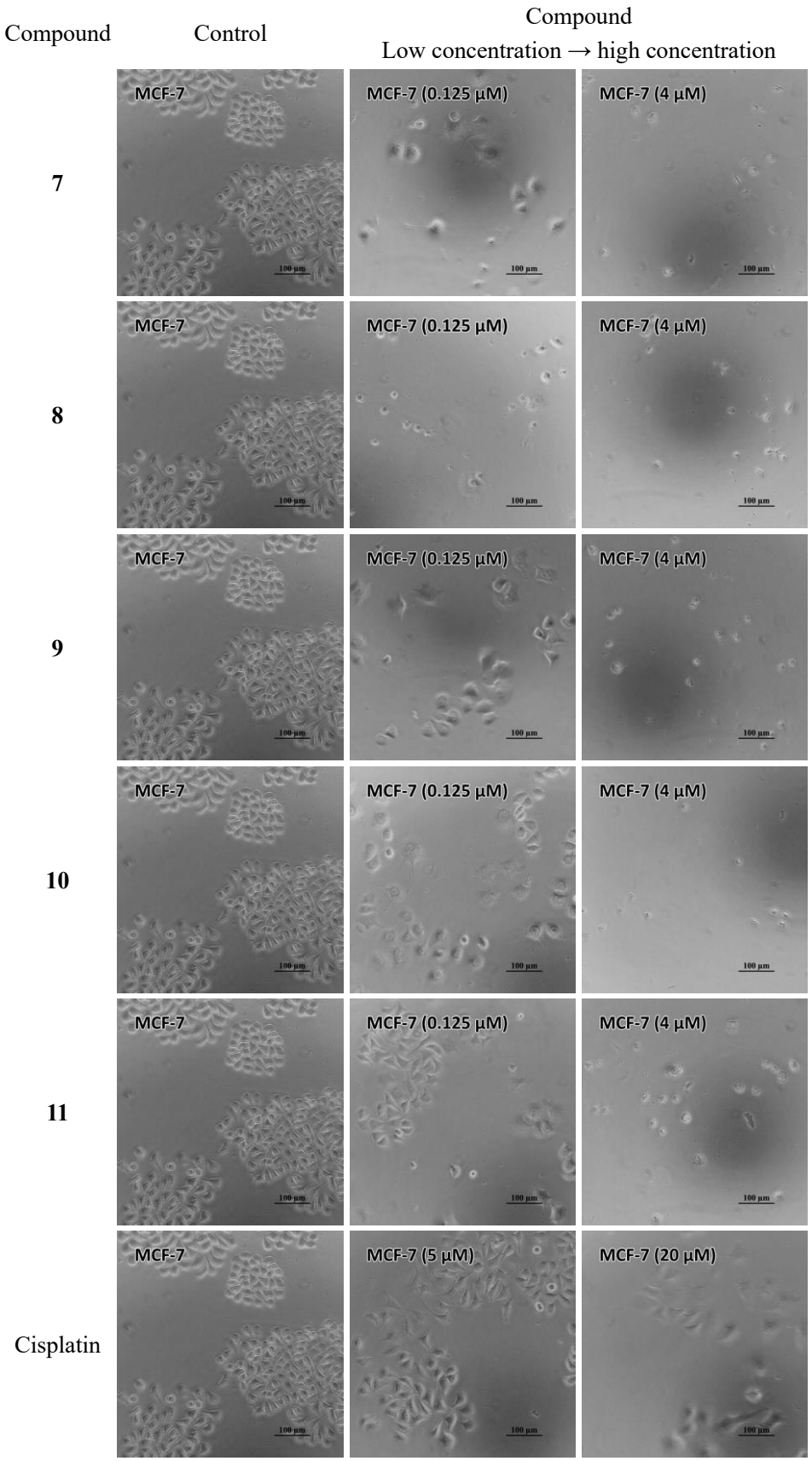


**Figure S44** The microscopic images of MCF-7 cells treated with increased concentrations of compounds **7**–**11** and cisplatin.

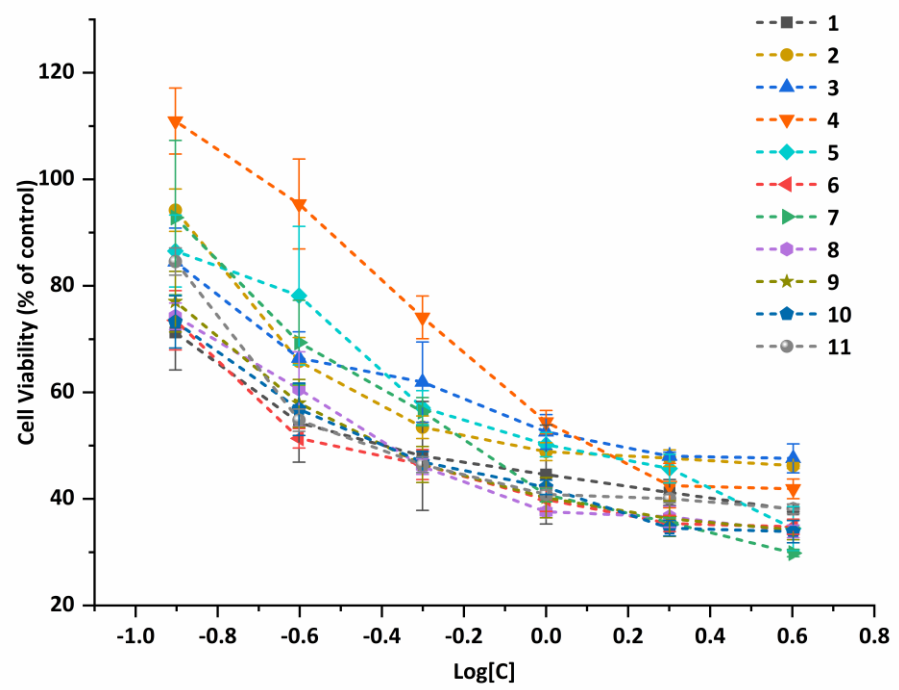


**Figure S45** The plots of cell viability *vs.* the concentration of compounds **1**–**11** against Bel-7402 cells.

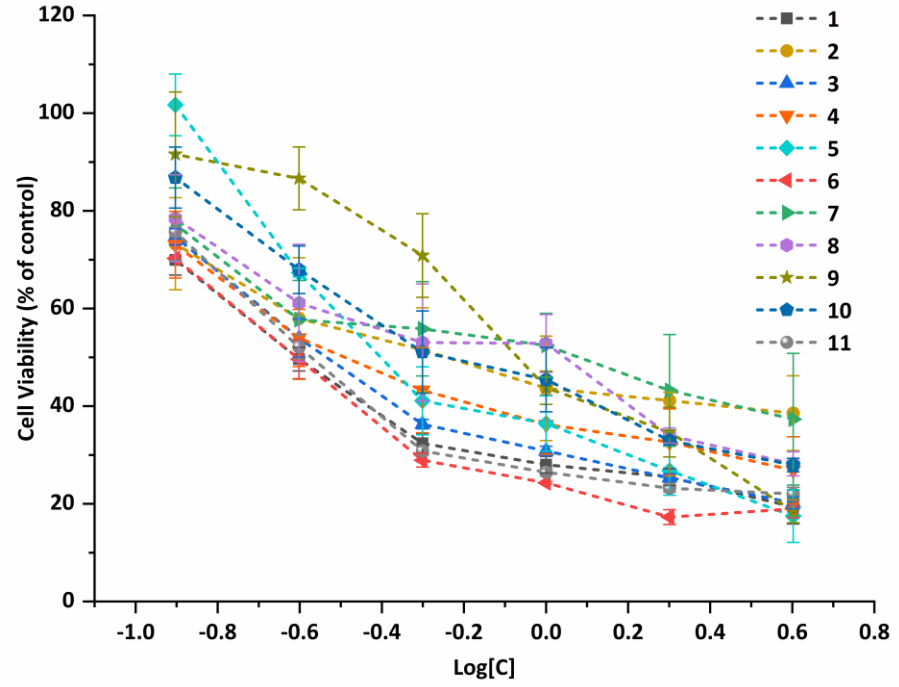


**Figure S46** The plots of cell viability *vs.* the concentration of compounds **1**–**11** against Eca-109 cells.

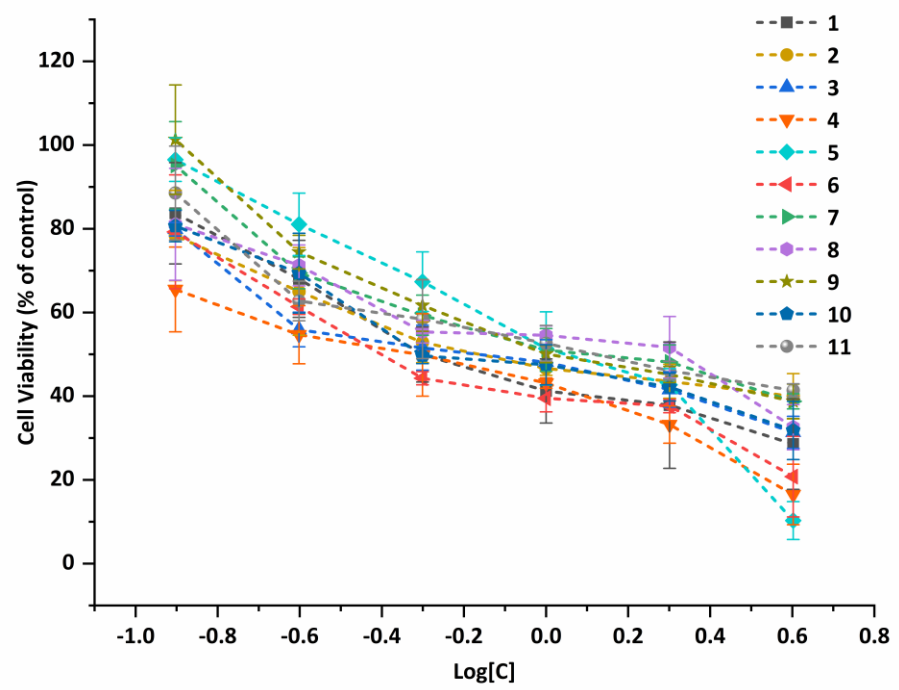


**Figure S47** The plots of cell viability *vs.* the concentration of compounds **1**–**11** against HeLa cells.

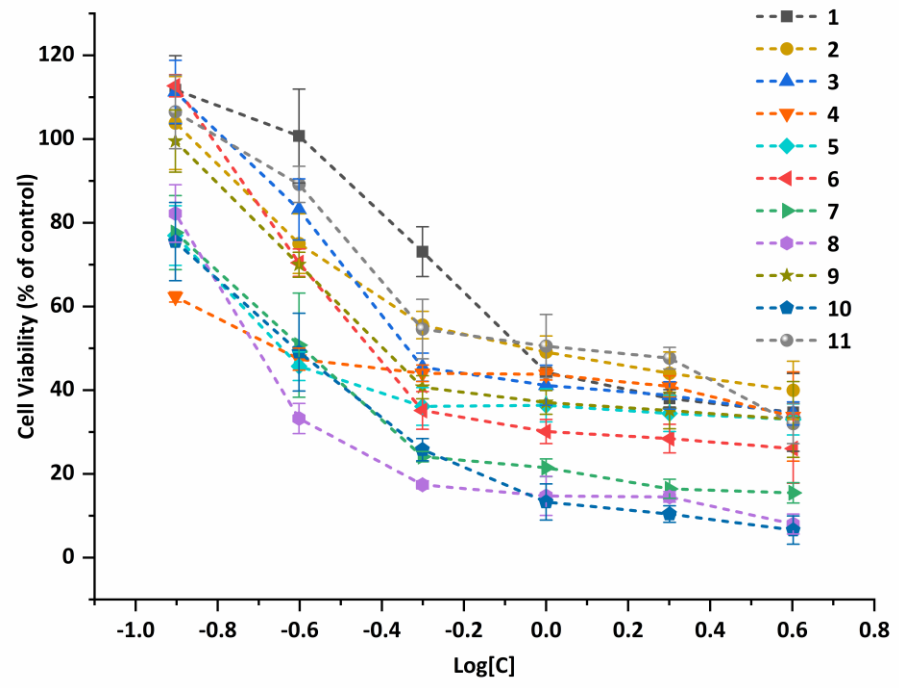


**Figure S48** The plots of cell viability *vs.* the concentration of compounds **1**–**11** against MCF-7 cells.

**Table S1** The CD sprctral bands and change ratios of CT-DNA and CT-DNA with compounds **1**–**11**: wavelength $\lambda$ (degree of ellipcity, $\Phi$)

| Conditions | $\lambda$/nm ($\Phi$/°) | | Change ratio (%) | |
|---|---|---|---|---|
| | (−) band | (+) band | (–) band | (+) band |
| 600 μM CT-DNA | 245(−6.84) | 276(5.37) | - | - |
| 600 μM CT-DNA | 247(−6.71) | 276(5.50) | - | - |
| 600 μM CT-DNA | 247(−6.81) | 278(5.84) | - | - |
| 600 μM CT-DNA + 60 μM compound **1** | 245(−5.45) | 277(5.88) | −20 | 9 |
| 600 μM CT-DNA + 120 μM compound **1** | 245(−5.02) | 278(5.75) | −27 | 7 |
| 600 μM CT-DNA + 180 μM compound **1** | 245(−3.62) | 279(5.35) | −47 | 0 |
| 600 μM CT-DNA + 240 μM compound **1** | 245(−2.73) | 280(4.75) | −60 | −12 |
| 600 μM CT-DNA + 300 μM compound **1** | 245(−2.16) | 280(3.91) | −68 | −27 |
| 600 μM CT-DNA + 60 μM compound **2** | 247(−5.37) | 278(6.01) | −20 | 9 |
| 600 μM CT-DNA + 120 μM compound **2** | 247(−4.81) | 279(6.37) | −28 | 16 |
| 600 μM CT-DNA + 180 μM compound **2** | 247(−4.12) | 280(6.33) | −39 | 15 |
| 600 μM CT-DNA + 240 μM compound **2** | 248(−2.97) | 280(5.46) | −56 | −1 |
| 600 μM CT-DNA + 300 μM compound **2** | 249(−2.55) | 281(5.35) | −62 | −3 |
| 600 μM CT-DNA + 60 μM compound **3** | 247(−5.57) | 277(5.29) | −17 | −4 |
| 600 μM CT-DNA + 120 μM compound **3** | 247(−4.62) | 277(5.09) | −31 | −7 |
| 600 μM CT-DNA + 180 μM compound **3** | 247(−4.06) | 278(4.10) | −39 | −25 |
| 600 μM CT-DNA + 240 μM compound **3** | 247(−3.09) | 280(3.17) | −54 | −42 |
| 600 μM CT-DNA + 300 μM compound **3** | 247(−2.34) | 281(3.01) | −65 | −45 |
| 600 μM CT-DNA + 60 μM compound **4** | 247(−4.61) | 277(4.76) | −31 | −13 |
| 600 μM CT-DNA +120 μM compound **4** | 247(−3.20) | 282(3.69) | −52 | −33 |
| 600 μM CT-DNA + 180 μM compound **4** | 247(−2.67) | 282(3.43) | −60 | −38 |
| 600 μM CT-DNA + 240 μM compound **4** | 249(−1.44) | 287(2.91) | −79 | −47 |
| 600 μM CT-DNA + 300 μM compound **4** | 255(−0.81) | 295(1.95) | −88 | −65 |
| 600 μM CT-DNA + 60 μM compound **5** | 245(−5.61) | 277(5.44) | −18 | 1 |
| 600 μM CT-DNA + 120 μM compound **5** | 245(−5.04) | 278(5.29) | −26 | −1 |
| 600 μM CT-DNA + 180 μM compound **5** | 245(−4.20) | 278(4.95) | −39 | −8 |
| 600 μM CT-DNA + 240 μM compound **5** | 245(−4.06) | 280(4.72) | −41 | −12 |
| 600 μM CT-DNA + 300 μM compound **5** | 245(−3.38) | 280(4.39) | −51 | −18 |
| 600 μM CT-DNA + 60 μM compound **6** | 247(−5.62) | 279(5.27) | −17 | −10 |
| 600 μM CT-DNA + 120 μM compound **6** | 247(−4.62) | 279(5.12) | −32 | −14 |
| 600 μM CT-DNA + 180 μM compound **6** | 247(−3.77) | 282(4.12) | −45 | −34 |
| 600 μM CT-DNA + 240 μM compound **6** | 248(−2.96) | 282(3.86) | −57 | −48 |
| 600 μM CT-DNA + 300 μM compound **6** | 248(−1.76) | 283(2.41) | −74 | −89 |
| 600 μM CT-DNA + 60 μM compound **7** | 245(−6.29) | 280(5.03) | −8 | −6 |
| 600 μM CT-DNA + 120 μM compound **7** | 246(−6.36) | 283(4.92) | −7 | −20 |
| 600 μM CT-DNA + 180 μM compound **7** | 247(−4.43) | 283(4.30) | −35 | −8 |
| 600 μM CT-DNA + 240 μM compound **7** | 247(−2.91) | 282(2.61) | −57 | −51 |
| 600 μM CT-DNA + 300 μM compound **7** | 249(−2.32) | 284(4.92) | −66 | −8 |
| 600 μM CT-DNA + 60 μM compound **8** | 247(−5.35) | 282(5.67) | −21 | −7 |
| 600 μM CT-DNA + 120 μM compound **8** | 247(−5.04) | 282(5.69) | −26 | −3 |
| 600 μM CT-DNA + 180 μM compound **8** | 247(−3.81) | 282(4.53) | −44 | −23 |
| 600 μM CT-DNA + 240 μM compound **8** | 247(−3.38) | 282(4.80) | −50 | −23 |
| 600 μM CT-DNA + 300 μM compound **8** | 248(−2.26) | 282(3.52) | −67 | −48 |
| 600 μM CT-DNA + 60 μM compound **9** | 247(−5.35) | 281(5.77) | −20 | 5 |
| 600 μM CT-DNA + 120 μM compound **9** | 247(−4.85) | 281(5.52) | −28 | 0 |
| 600 μM CT-DNA + 180 μM compound **9** | 247(−4.57) | 281(5.22) | −32 | −5 |
| 600 μM CT-DNA + 240 μM compound **9** | 247(−3.87) | 283(4.83) | −42 | −12 |
| 600 μM CT-DNA + 300 μM compound **9** | 248(−2.65) | 285(2.82) | −61 | −49 |
| 600 μM CT-DNA + 60 μM compound **10** | 247(−5.51) | 278(5.89) | −18 | 7 |
| 600 μM CT-DNA + 120 μM compound **10** | 247(−5.48) | 279(5.35) | −18 | −3 |

| | | | | |
|---|---|---|---|---|
| 600 μM CT-DNA + 180 μM compound **10** | 247(−3.37) | 280(4.97) | −50 | −10 |
| 600 μM CT-DNA + 240 μM compound **10** | 247(−2.66) | 281(3.96) | −60 | −28 |
| 600 μM CT-DNA + 300 μM compound **10** | 249(−2.06) | 282(3.31) | −69 | −40 |
| 600 μM CT-DNA + 60 μM compound **11** | 245(−5.36) | 277(6.28) | −22 | 17 |
| 600 μM CT-DNA + 120 μM compound **11** | 245(−4.85) | 280(6.35) | −29 | 18 |
| 600 μM CT-DNA + 180 μM compound **11** | 245(−3.86) | 282(6.44) | −44 | 20 |
| 600 μM CT-DNA + 240 μM compound **11** | 245(−3.60) | 282(5.96) | −47 | 11 |
| 600 μM CT-DNA + 300 μM compound **11** | 245(−3.05) | 282(5.64) | −55 | 5 |

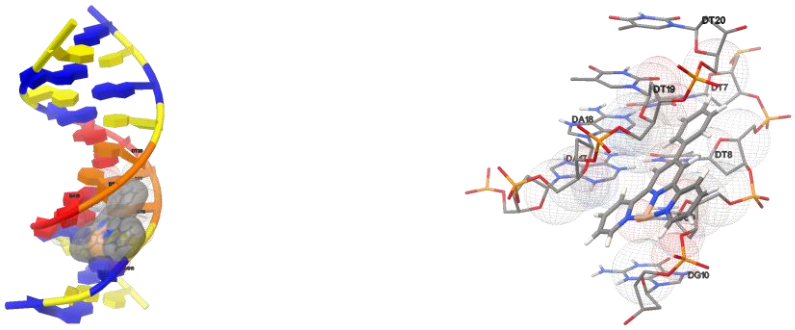


**Figure S49** The most favorable orientation of compound **1** with the minor groove of the B-DNA (PDB ID: 1BNA[1]).

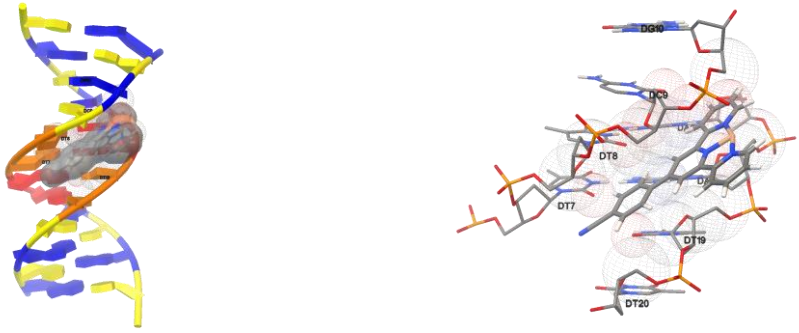


**Figure S50** The most favorable orientation of compound **2** with the minor groove of the B-DNA (PDB ID: 1BNA).

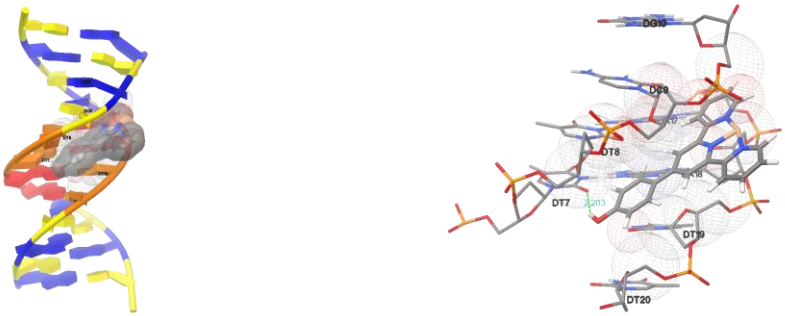


**Figure S51** The most favorable orientation of compound **3** with the minor groove of the B-DNA (PDB ID: 1BNA).

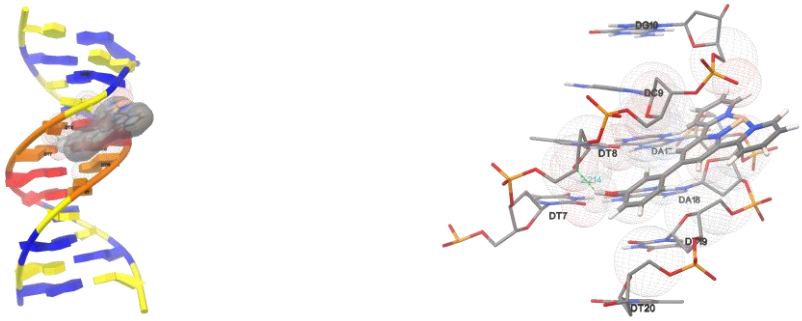


**Figure S52** The most favorable orientation of compound **4** with the minor groove of the B-DNA (PDB ID: 1BNA).

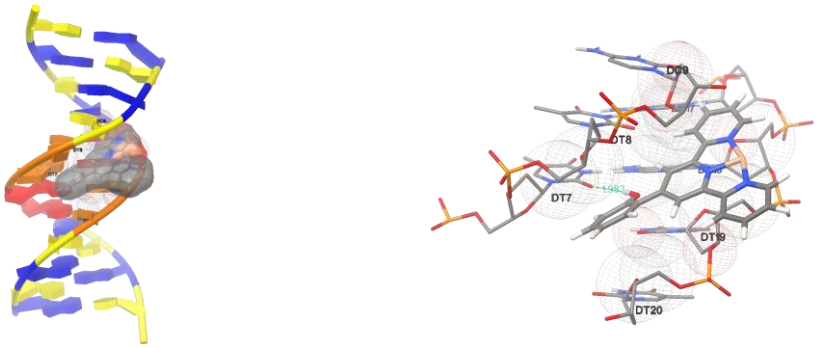


**Figure S53** The most favorable orientation of compound **5** with the minor groove of the B-DNA (PDB ID: 1BNA).

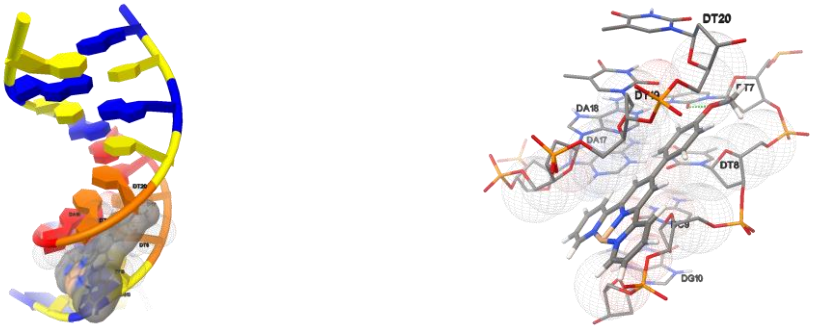


**Figure S54** The most favorable orientation of compound **6** with the minor groove of the B-DNA (PDB ID: 1BNA).

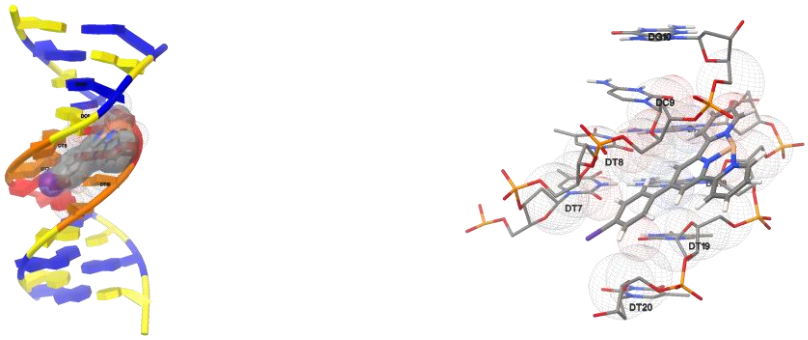


**Figure S55** The most favorable orientation of compound **7** with the minor groove of the B-DNA (PDB ID: 1BNA).

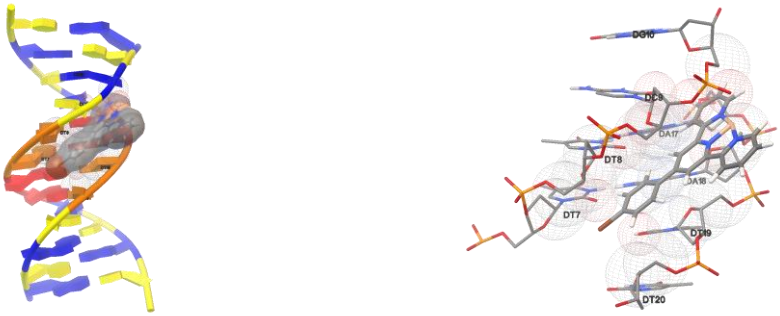


**Figure S56** The most favorable orientation of compound **8** with the minor groove of the B-DNA (PDB ID: 1BNA).


**Figure S57** The most favorable orientation of compound **9** with the minor groove of the B-DNA (PDB ID: 1BNA).

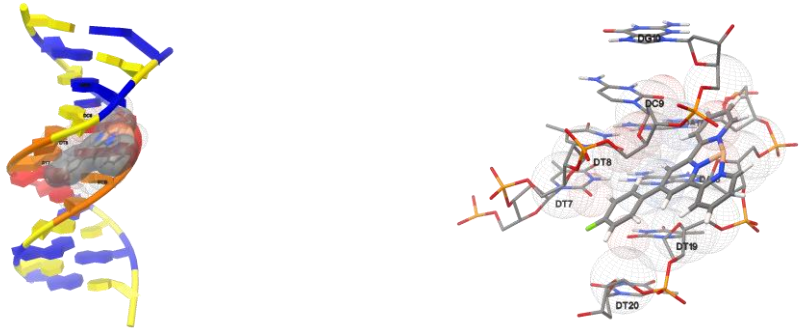


**Figure S58** The most favorable orientation of compound **10** with the minor groove of the B-DNA (PDB ID: 1BNA).

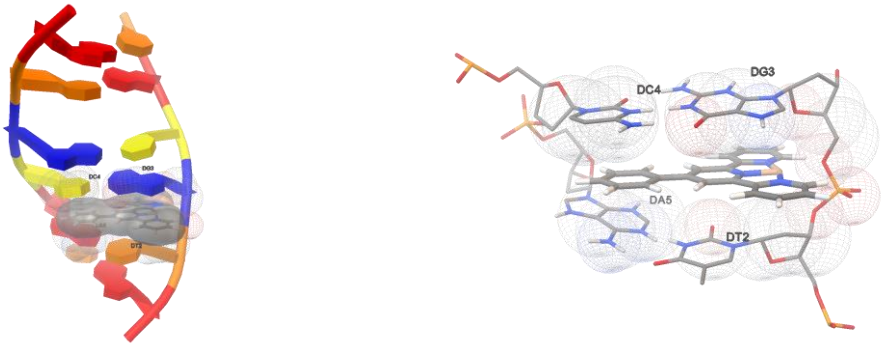


**Figure S59** The most favorable orientation of compound **1** intercalating with the DNA (PDB ID: 4JD8[2]).

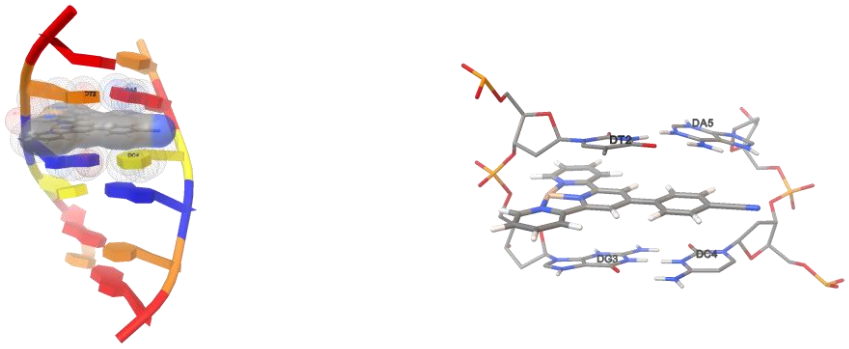


**Figure S60** The most favorable orientation of compound **2** intercalating with the DNA (PDB ID: 4JD8).

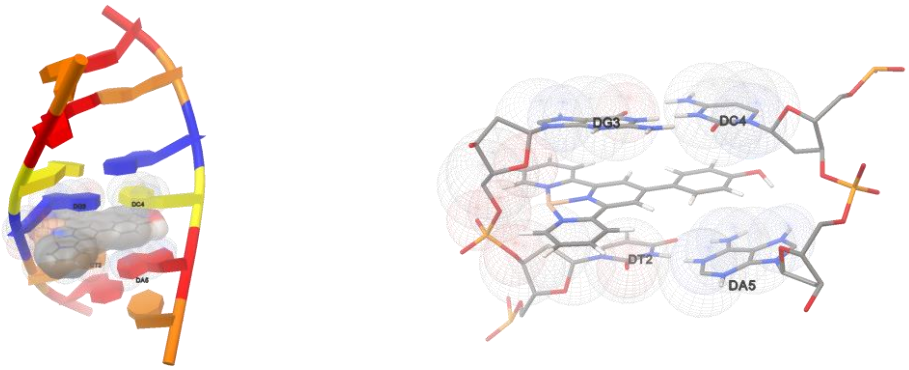


**Figure S61** The most favorable orientation of compound **3** intercalating with the DNA (PDB ID: 4JD8).

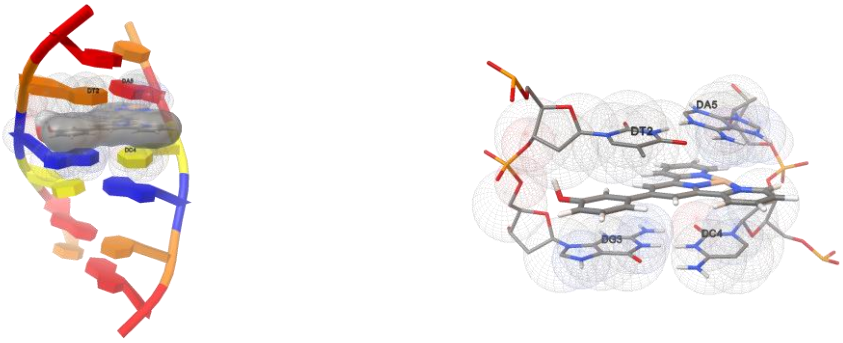


**Figure S62** The most favorable orientation of compound **4** intercalating with the DNA (PDB ID: 4JD8).

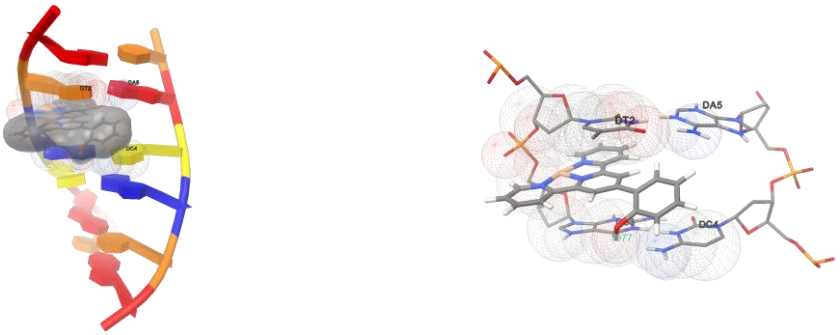


**Figure S63** The most favorable orientation of compound **5** intercalating with the DNA (PDB ID: 4JD8).

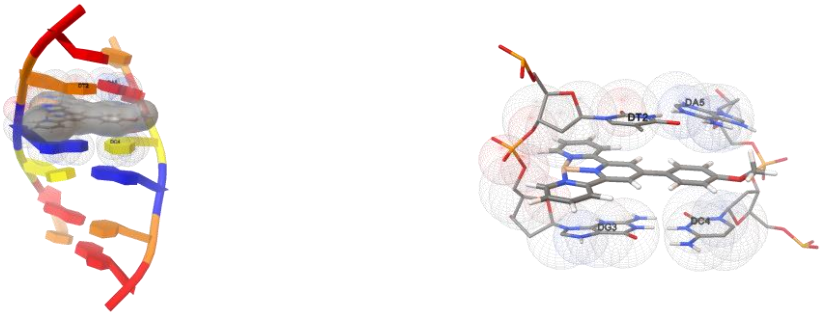


**Figure S64** The most favorable orientation of compound **6** intercalating with the DNA (PDB ID: 4JD8).

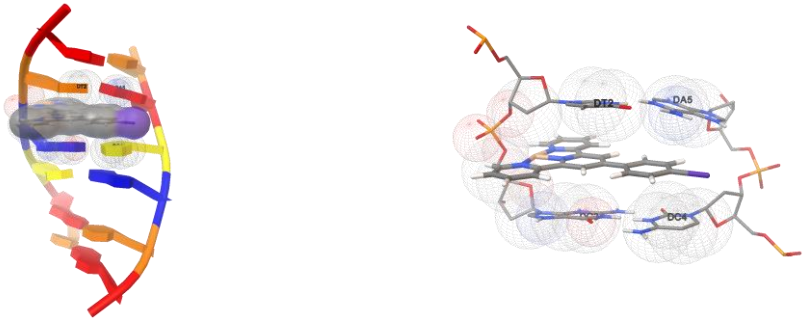


**Figure S65** The most favorable orientation of compound **7** intercalating with the DNA (PDB ID: 4JD8).

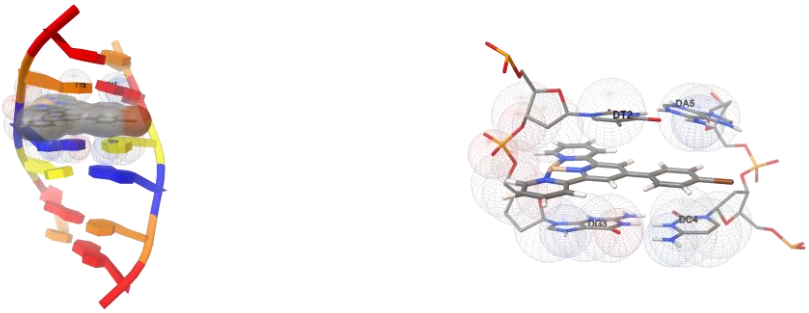


**Figure S66** The most favorable orientation of compound **8** intercalating with the DNA (PDB ID: 4JD8).

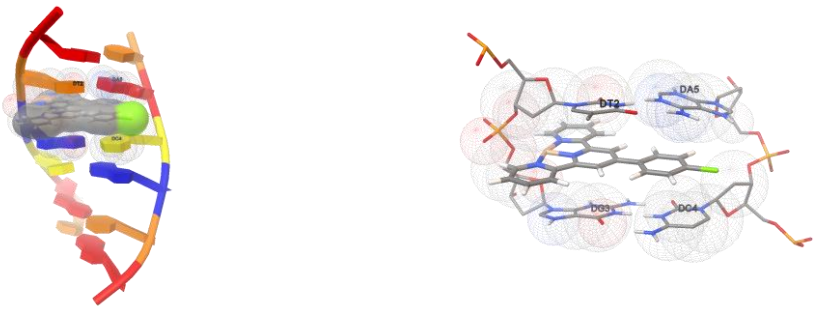


**Figure S67** The most favorable orientation of compound **9** intercalating with the DNA (PDB ID: 4JD8).

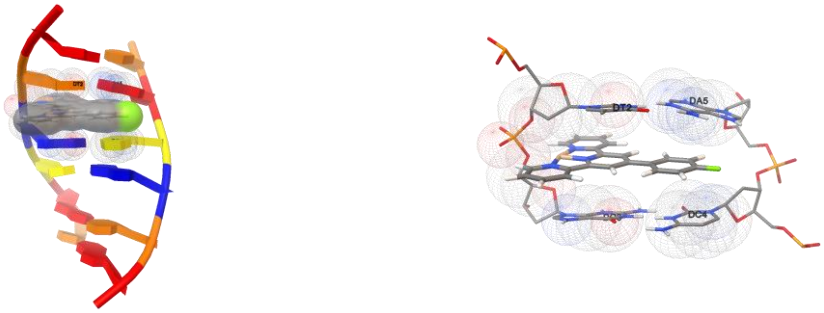


**Figure S68** The most favorable orientation of compound **10** intercalating with the DNA (PDB ID: 4JD8).

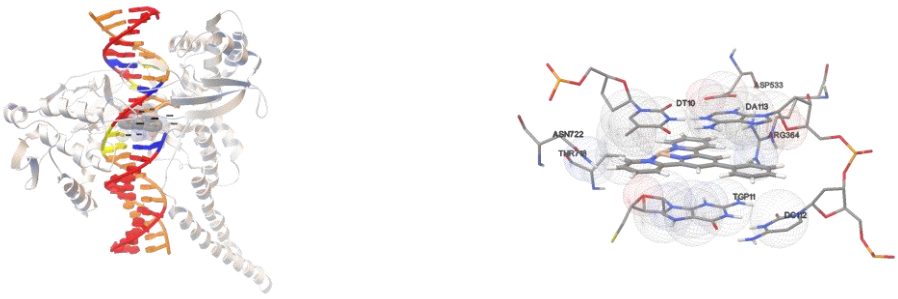


**Figure S69** Molecular docking models of **1** in the active site of DNA–Topo I complex (PDB ID: 1SC7[3]).

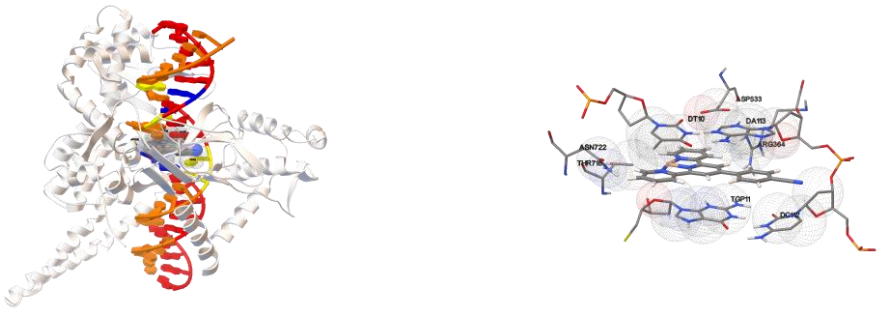


**Figure S70** Molecular docking models of **2** in the active site of DNA–Topo I complex (PDB ID: 1SC7).

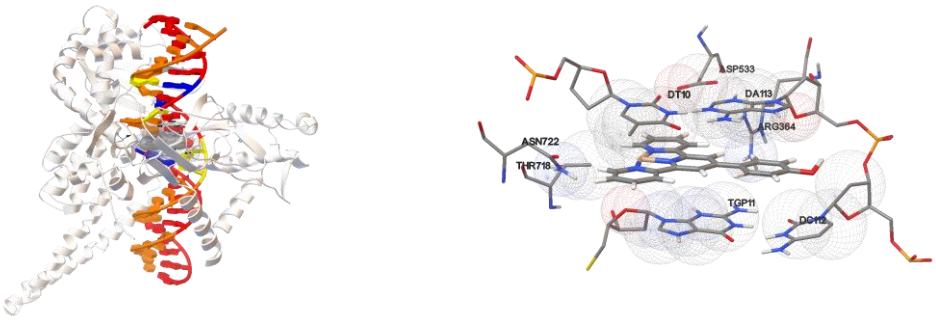


**Figure S71** Molecular docking models of **3** in the active site of DNA–Topo I complex (PDB ID: 1SC7).


**Figure S72** Molecular docking models of **4** in the active site of DNA–Topo I complex (PDB ID: 1SC7).

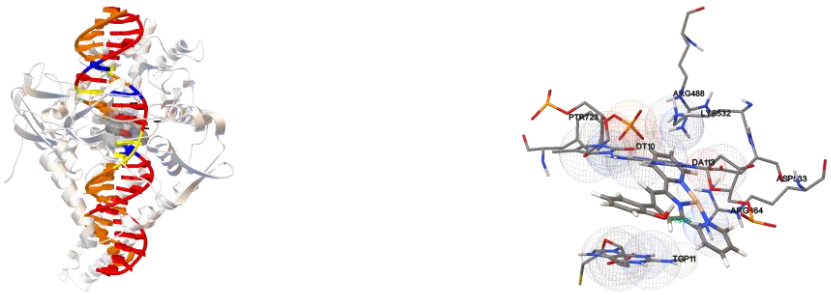

**Figure S73** Molecular docking models of **5** in the active site of DNA–Topo I complex (PDB ID: 1SC7).

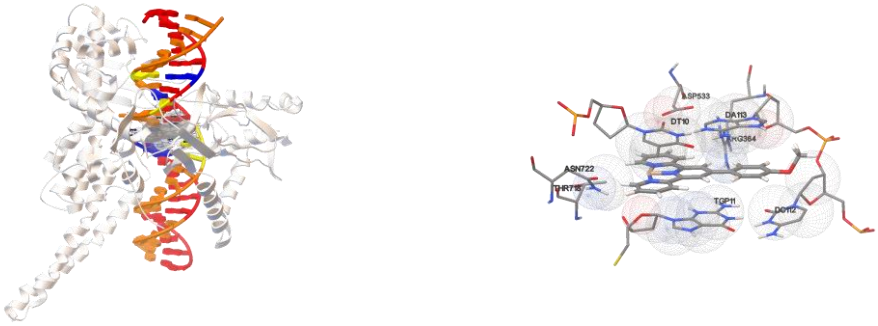

**Figure S74** Molecular docking models of **6** in the active site of DNA–Topo I complex (PDB ID: 1SC7).

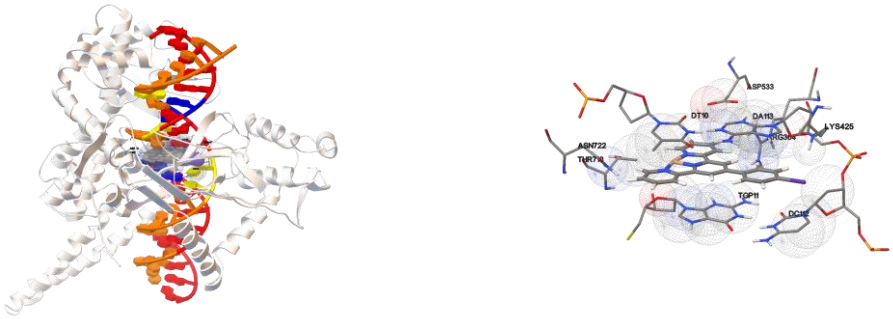

**Figure S75** Molecular docking models of **7** in the active site of DNA–Topo I complex (PDB ID: 1SC7).

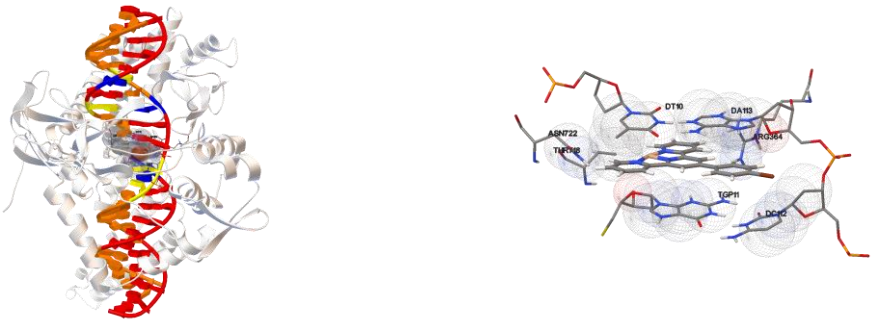

**Figure S76** Molecular docking models of **8** in the active site of DNA–Topo I complex (PDB ID: 1SC7).

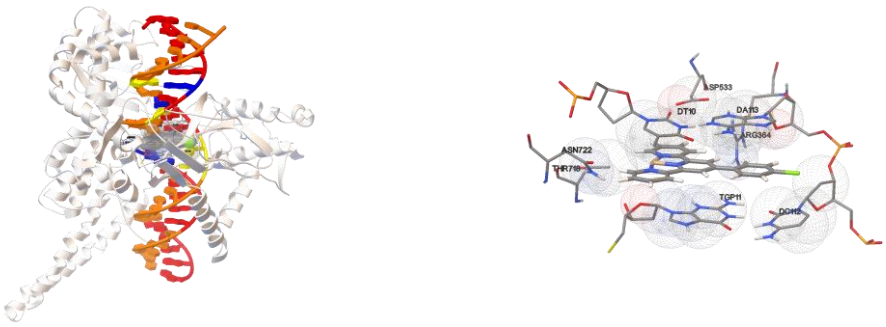


**Figure S77** Molecular docking models of **9** in the active site of DNA–Topo I complex (PDB ID: 1SC7).

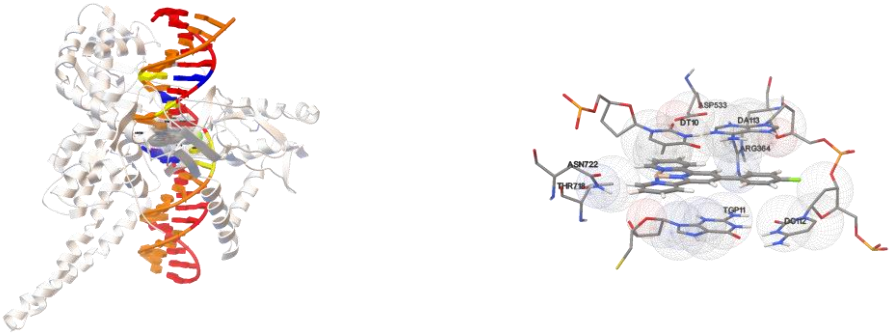


**Figure S78** Molecular docking models of **10** in the active site of DNA–Topo I complex (PDB ID: 1SC7).

## References


1. H. R. Drew, R. M. Wing, T. Takano, C. Broka, S. Tanaka, K. Itakura and R. E. Dickerson, *Proc. Natl. Acad. Sci. U.S.A.*, 1981, **78**, 2179–2183.
2. J. P. Hall, D. Cook, S. R. Morte, P. McIntyre, K. Buchner, H. Beer, D. J. Cardin, J. A. Brazier, G. Winter and C. J. Cardin, *J. Am. Chem. Soc.*, 2013, **135**, 12652–12659.
3. B. L. Staker, M. D. Feese, M. Cushman, Y. Pommier, D. Zembower, L. Stewart and A. B. Burgin, *J. Med. Chem.*, 2005, **48**, 2336–2345.